Journal of Medicinal Chemistry

pubs.acs.org/jmc

Article

A Novel N-Substituted Valine Derivative with Unique Peroxisome Proliferator-Activated Receptor γ Binding Properties and Biological Activities

Franck Peiretti,*,▽ Roberta Montanari,▽ Davide Capelli, Bernadette Bonardo, Cécilia Colson, Ez-Zoubir Amri, Marina Grimaldi, Patrick Balaguer, Keiichi Ito, Robert G. Roeder, Giorgio Pochetti,▽ and Jean Michel Brunel▽

Cite This: https://dx.doi.org/10.1021/acs.jmedchem.0c01555

Read Online

ACCESS | Metrics & More | Article Recommendations | Supporting Information

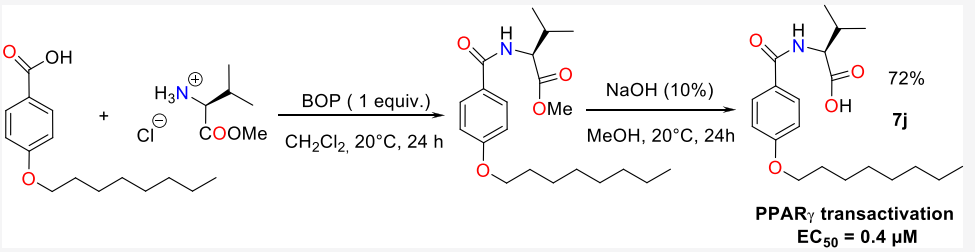

ABSTRACT: A proprietary library of novel *N*-aryl-substituted amino acid derivatives bearing a hydroxamate head group allowed the identification of compound **3a** that possesses weak proadipogenic and peroxisome proliferator-activated receptor γ (PPARγ) activating properties. The systematic optimization of **3a**, in order to improve its PPARγ agonist activity, led to the synthesis of compound **7j** (*N*-aryl-substituted valine derivative) that possesses dual PPARγ/PPARα agonistic activity. Structural and kinetic analyses reveal that **7j** occupies the typical ligand binding domain of the PPARγ agonists with, however, a unique high-affinity binding mode. Furthermore, **7j** is highly effective in preventing cyclin-dependent kinase 5-mediated phosphorylation of PPARγ serine 273. Although less proadipogenic than rosiglitazone, **7j** significantly increases adipocyte insulin-stimulated glucose uptake and efficiently promotes white-to-brown adipocyte conversion. In addition, **7j** prevents oleic acid-induced lipid accumulation in hepatoma cells. The unique biochemical properties and biological activities of compound **7j** suggest that it would be a promising candidate for the development of compounds to reduce insulin resistance, obesity, and nonalcoholic fatty liver disease.

INTRODUCTION

Peroxisome proliferator-activated receptors (PPARs) are transcription factors belonging to the nuclear receptor superfamily and activated by ligands such as dietary fatty acids, particularly polyunsaturated fatty acids. The three PPAR subtypes: PPARα, PPARγ, and PPARδ (β), have different, yet overlapping, tissue expression patterns[1] and exert major roles in the regulation of specific physiological functions including glucose and lipid metabolism and energy homeostasis.[2−4] These features make PPARs important molecular targets for the development of drugs for metabolic diseases.

PPARα is expressed in all metabolic tissues but predominantly in the liver where it is involved in the regulation of the uptake and oxidation of fatty acids and lipoprotein metabolism.[5] The fibrate family of drugs (clofibrate and fenofibrate) is pharmacologically weak agonists of PPARα that are used to treat dyslipidemia as they lower plasma triglycerides and increase high-density lipoprotein cholesterol levels.[6] The PPARα agonist fenofibrate has also a beneficial effect in patient with nonalcoholic fatty liver disease (NAFLD) characterized by the accumulation of triglycerides in hepatocytes.[7] However, fibrates increase markers of cardiovascular and renal disease and that of liver dysfunction, which underlines their ability to trigger adverse effects.[8] Therefore, efforts are being made to develop PPARα agonists with improved clinical efficacy, penafibrate being one of these new generation agonists.[9]

PPARδ is involved in the regulation of fatty acid oxidation and mitochondrial respiration predominantly in skeletal muscle, liver, and adipose tissue.[10] Therefore, agonists targeting PPARδ may be considered as potential therapeutic agents for insulin resistance-related conditions. PPARδ

Received: September 6, 2020

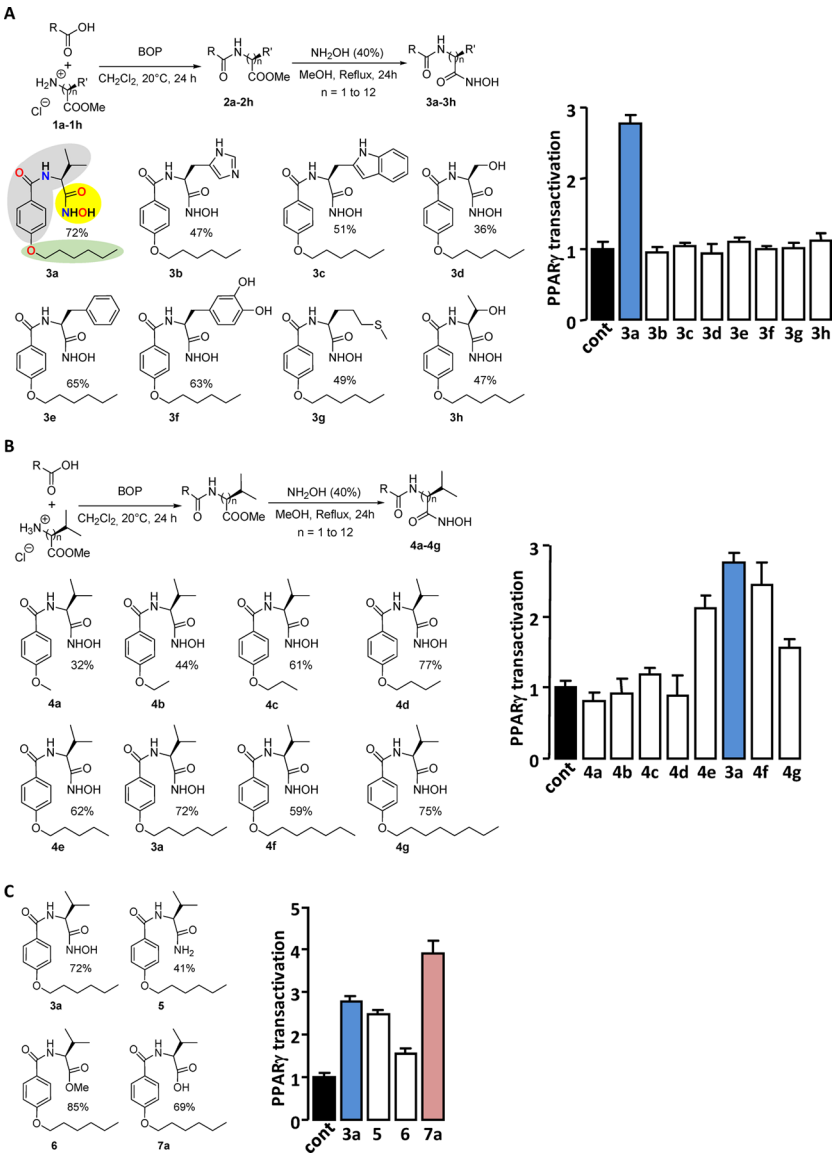

Figure 1. Chemical structures and PPARγ agonist activity of **3a** and its derivatives. (A) Amino acid core, (B) hydrophobic capping group, and (C) binding head group of **3a** were modified (left panels), and PPARγ transactivation activity of each molecule (5 μM) was measured (right panels). Color fills accentuate the amino acid core (gray), hydrophobic capping group (green), and binding head group (yellow) of **3a**. The percentage indicates the yield of the synthesis. PPARγ transactivation values are means ± SD expressed relative to the mean of control values, which was set to 1.

agonists have been developed and used in research,[11] but none of them are currently approved for clinical use.

PPARγ is considered the master regulator of adipogenesis via its promotion of lipid production and storage. Thiazolidinediones, including rosiglitazone (Rosi) and pioglitazone, are the most effective PPARγ activating drugs that were widely prescribed for the treatment of type 2 diabetes.[12] However, their strong agonist activities are partly responsible for unwanted harmful side effects such as weight gain, fluid retention, osteoporosis, heart failure, and cancer,[13,14] which precipitated their withdrawal from the market.

The quest for antidiabetic compounds targeting PPAR with good therapeutic potential and reduced adverse effects has followed two main directions. The one based on the observation that a moderate, rather than full, activation of PPARγ dissociates the deleterious from the therapeutic effects of the agonist has led to the generation of selective PPARγ modulators (SPPARγMs) with higher therapeutic profiles than full agonists.[15,16] The peculiar properties of SPPARγM are being explained by the ability of PPARγ to adopt ligand-specific conformations with different transcriptional signatures. In addition, it has been shown that the clinical benefit of PPARγ partial agonists and SPPARγMs also involves their ability to inhibit the cyclin-dependent kinase 5 (CDK5)-mediated PPARγ phosphorylation at serine 273.[17,18] The other concept for developing safe antidiabetic drugs targeting PPAR considers that beneficial effects of their activation could counteract their harmful effects. PPARα/γ dual agonists, so-called glitazars, that combine the insulin sensitizing effect of PPARγ agonists with the beneficial effect of PPARα agonists on the lipid profile are representative of this class of drugs.[19,20] Saroglitazar is approved in India for the treatment of peculiar type of diabetic dyslipidemia and hypertriglyceridemia.[21,22] Moreover, dual α/δ and γ/δ PPAR agonists as well as "pan"

https://dx.doi.org/10.1021/acs.jmedchem.0c01555
J. Med. Chem. XXXX, XXX, XXX−XXX

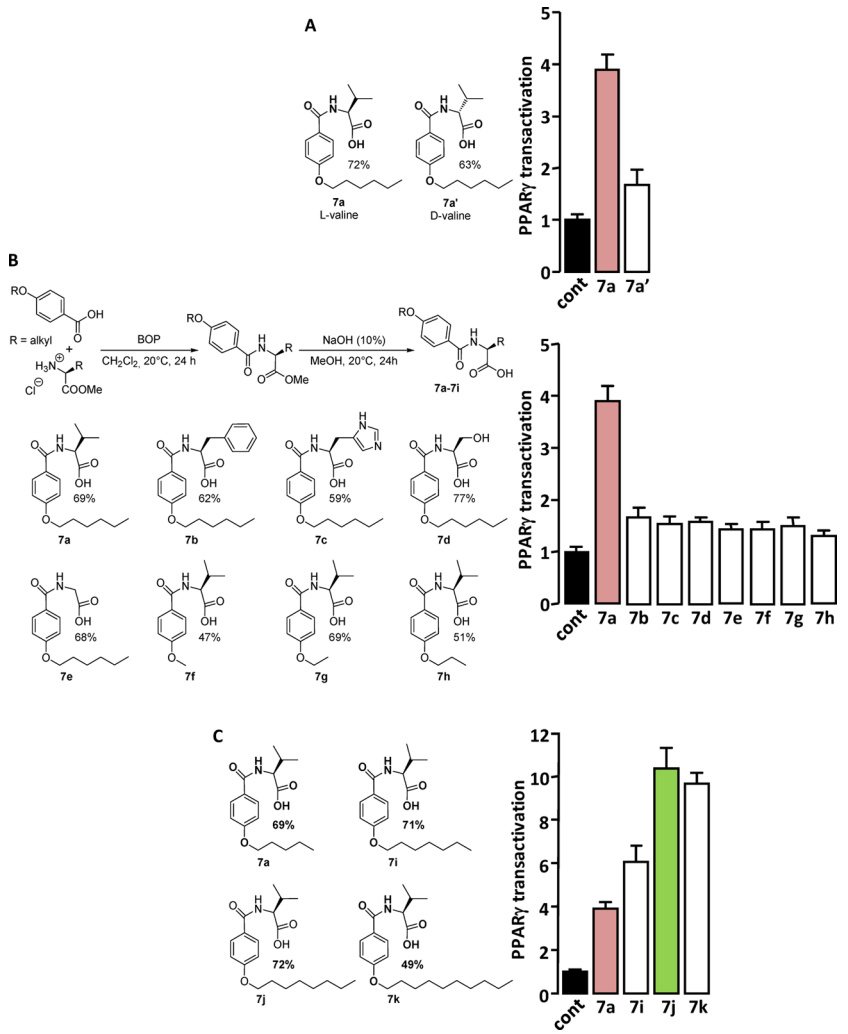

Figure 2. Chemical structures and PPARγ agonist activity of **7a** and its derivatives. (A–C) Absolute conformations of the valine core (A), the amino acid core (B), or the hydrophobic capping group (C) of **7a** were modified (left panels), and PPARγ transactivation activity of each molecule (5 μM) was measured (right panels). The percentage indicates the yield of the synthesis. PPARγ transactivations are expressed as shown in Figure 1.

agonists acting on all three isoforms are the subject of intense investigations[23−25] that could lead to the generation of molecules with potential additional therapeutic indications.

This work reports a mild two-step synthesis of a library of new *N*-aryl-substituted amino acid derivatives from commercially easily available and inexpensive reagents. The effect of these compounds, in particular the influence of substitutions on their phenyl group, was evaluated on PPAR activity and led to the development of a new balanced and potent dual PPARα/γ agonist with unique ligand binding properties and singular biological activities that would be expected for a potential therapeutic candidate to reduce insulin resistance, obesity, and NAFLD.

RESULTS AND DISCUSSION

New *N*-aryl-substituted amino acid derivatives bearing a hydroxamate head group (head), initially designed to identify MMP inhibitors, were screened on their ability to induce spontaneous (in the absence of any other inductor) adipocyte differentiation of 3T3-L1 cells by measuring intracellular lipid accumulation. The molecule named **3a** (4-hexyloxy-*N*-((*S*)-1-hydroxycarbamoyl-2-methyl-propyl)-benzamide), which contains an L-valine (core) and a six-carbon atom chain (capping group) (Figure 1A and Figure S1), was identified as a weak activator of adipocyte differentiation as compared with Rosi (Figure S2). We hypothesized that **3a** increased adipocyte differentiation by activating the master regulator of adipogenesis: PPARγ. The PPARγ agonistic activity of **3a** was confirmed by the use of a luminescence-based cell-based PPARγ transactivation assay in which a wild-type PPARγ ligand binding domain (PPARγ-*LBD*) is fused to the GAL4 DNA binding domain (*PPARγ-LBD-GAL4*) and the Firefly luciferase reporter gene is under the control of GAL4 binding elements (Figure 1A). Importantly, **3a** increased PPARγ activity by a factor of 2.8, while 1 μM Rosi (a full PPARγ agonist) increased it by a factor of 25 ± 7. A thorough comparison of the PPARγ activation properties of the newly synthesized compounds with that of Rosi will be carried out at the later stage. We initiated a process to identify the domains of **3a** involved in PPARγ activation that would ideally lead to an optimization of its PPARγ agonist activity.

Effect of the Amino Acid Core. Analogues of the **3a** hit were designed and synthesized through a reaction involving a two-step synthesis procedure in dichloromethane from amino

https://dx.doi.org/10.1021/acs.jmedchem.0c01555
J. Med. Chem. XXXX, XXX, XXX−XXX

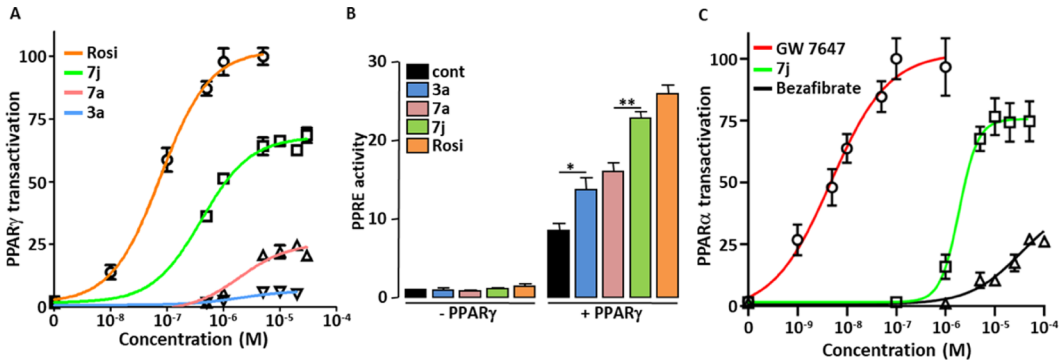

Figure 3. PPAR agonist activity of **3a**, **7a**, and **7j**. (A) Concentration-dependent PPARγ transactivation activities of **3a**, **7a**, and **7j** were compared to that of Rosi using the *PPARγ-LBD-GAL4* chimera assay. Values are means ± SD expressed as % of the maximal response measured with Rosi (5 μM). (B) HEK293 cells were transfected with PPRE-driven Firefly luciferase and SV40-driven Renilla luciferase coding vectors together with an empty plasmid (−PPARγ) or with the PPARγ expression vector (+PPARγ). After 36 h of post-transfection, cells were incubated for 17 h with **3a**, **7a**, **7j** (1 μM), or Rosi (0.1 μM). PPRE promoter activity was calculated as the ratio of Firefly/Renilla luciferase. Values are means ± SD expressed relative to the control situation (*p < 0.05 and **p < 0.01 (one-way ANOVA followed by Bonferroni's post-hoc test). (C) Concentration-dependent PPARα transactivation activities of **7j**, GW 7647, and bezafibrate were measured using the *PPARα-LBD-GAL4* chimera assay. Values are means ± SD expressed as % of the maximal response measured with GW 7647 (1 μM).

acid methyl ester hydrochloride **1a**−**1h**, easily prepared from amino acids. By using a BOP reagent as an efficient and versatile reagent for the coupling of alkyloxybenzoic acid with **1a**−**1h**, the synthesis of various substituted amino acid ester derivatives **2a**−**2h** in high chemical yields of up to 90% was achieved. It is noteworthy that the transient ester species are successfully transformed into their corresponding hydroxamic acid parent derivatives **3a**−**3h** by using hydroxylamine (40% H_2O) in MeOH at reflux for 24 h in yields varying from 36 to 72% (Figure 1A). Changing the L-valine core by any other amino acid decreased the PPARγ activation potency of the molecule (Figure 1A) perhaps due to the larger steric hindrance generated by the isopropyl moiety with respect to a benzyl or hydroxy methyl group.

Effect of the Carbon Atom Chain Capping Group. The different derivatives **4a**−**4h** were synthesized according to a similar procedure than for compounds **3a**−**3h** in good-to-excellent yields, varying from 32 to 75% (Figure 1B). Altering the number of carbons in the polycarbon chain capping group of the aryl moiety showed that a linear six-carbon chain was optimal for PPARγ activation (Figure 1B). This result suggests that the steric hindrance and the hydrophobic nature of the polycarbon chain are important factors to consider when designing most potent analogues.

Effect of the Head Group. Substitution of the hydroxamate head moiety in **3a** (Figure 1C) revealed that the preferred functions for PPARγ activation are OH > NHOH ≥ NH_2 > COOMe (Figure 1C). The analogue of **3a**, with a carboxylic acid moiety in place of the hydroxamate head group that optimally activated PPARγ, was named **7a** (Figure S3).

Optimization of PPARγ Agonist Activity of 7a. Changing the absolute conformation of the core valine from L to D abolished the PPARγ activation capacity of **7a** (Figure 2A). Furthermore, substitution of the amino acid core (L-valine) by other amino acid (L-form) and/or reducing the length of the polycarbon chain decreased the PPARγ activation efficiency of **7a** (Figure 2B). The PPARγ transactivation activity of **7a** was gradually enhanced by the extension of the polycarbon chain up to eight carbon atoms (Figure 2C). The analogue of **7a** with the eight-carbon atom chain in place of the six-carbon atom chain, which optimally activates PPARγ, was named **7j** (Figure S4). It should be noted that the presence of a chain with 10 carbon atoms in the molecule **7k** did not further enhance its ability to activate PPARγ.

Typical PPAR agonists are known to consist of three parts: a polar head group (usually bearing a carboxylic acid functionality), a hydrophobic tail moiety, and a linker, which consists of flexible methylene units and an aromatic ring.[26] Interestingly, **7a** and **7j** closely meet these elementary criteria.

Potency and Efficacy of PPARγ Activation. The concentration-dependent activation of PPARγ by the "hit" compound **3a** and its two "lead" derivatives **7a** and **7j** was compared to that of the PPARγ full agonist Rosi using the *PPARγ-LBD-GAL4* chimera assay (Figure 3A).

The potencies of the compounds were ranked as follows: **3a** ≈ **7a** < **7j** < Rosi (Table 1). Regarding their efficacy (maximal PPARγ transactivation), compounds were ranked as follows: **3a** < **7a** < **7j** ≤ Rosi (Table 1).

Table 1. EC_{50} and Maximal Activation of PPARγ and PPARα[a]

compound	PPAR	EC_{50} (nM)	activity (%)
Rosi	γ	76 ± 30	100
7j	γ	400 ± 150	66.36 ± 3.41
7a	γ	1940 ± 940	25.06 ± 2.03
3a	γ	1840 ± 1020	6.33 ± 1.03
GW 7647	α	5.4 ± 1	100
7j	α	1882 ± 665	75.6 ± 3.83
bezafibrate	α	31,700 ± 5410	35.4 ± 3.81

[a]Activities are expressed as % of the maximal response measured with 5 μM Rosi (for PPARγ) or with 1 μM GW 7647 (for PPARα). Values are means ± SD.

PPARγ activation elicited by **7j** was around 66% of that obtained with Rosi. However, this value is certainly overestimated. Indeed, in this specific cell-based assay, we observed that the Renilla luciferase expression (Figure S5A), which is used to normalize reporter gene values for variations inherent to transfection efficiency and sample handling, was more reduced by **7j** concentrations that induce maximal

https://dx.doi.org/10.1021/acs.jmedchem.0c01555
J. Med. Chem. XXXX, XXX, XXX−XXX

PPARγ activity (>10^{-6} M) than by Rosi. As a consequence, inclusion of Renilla luciferase expression values in the calculation of PPARγ activation by **7j** leads to an "artificial rise" of the maximum response (Figure S5B). Interestingly, the measurement of ATP cell content revealed that the number of viable HEK293 cells was no more reduced by **7j** than by Rosi, ruling out that the **7j**-dependent decrease in Renilla luciferase expression is due to a reduction in the number of viable cells (Figure S5C).

Taken together, these data allow us to define **3a** and **7a** as partial agonists of PPARγ and **7j** as a strong partial agonist of PPARγ.

A PPAR responsive element (PPRE)-based luciferase assay was carried out to assess the ability of **3a**, **7a**, and **7j** to transactivate genes controlled by the binding of PPARγ to PPRE. The three molecules increased the expression of PPRE-driven luciferase only when full-length PPARγ was expressed (Figure 3B), showing that these molecules stimulate the actual transcriptional activity of PPARγ. Interestingly, the transactivation efficiencies were in agreement with those measured by the *PPARγ-LBD-GAL4* chimera assay, i.e., **3a** ≈ **7a** < **7j**. In addition, and as expected, 1 μM **7j** and 0.1 μM Rosi gave similar activation levels in both the *PPARγ-LBD-GAL4* chimera assay and PPRE-based assay.

To attest that **3a**, **7a**, and **7j** are actual PPARγ ligands, their binding affinity (K_d) and rate constants (k_{on} and k_{off}) for PPARγ were compared to those of the reference ligand Rosi by surface plasmon resonance technology-based experiments (Table 2 and Figure S6).

Table 2. Affinity (K_d) and Rate Constants (k_{on} and k_{off}) for PPARγ/Ligand and PPARα/Ligand Interactions[a]

interaction	k_{on} (M^{-1} s^{-1})	k_{off} (s^{-1})	K_d (nM)
PPARγ/Rosi	3.45 (0.02) × 10^5	0.0164 (0.0001)	47.6 (0.3)
PPARγ/**7j**	5.65 (0.06) × 10^5	0.0170 (0.0001)	30.1 (0.3)
PPARγ/**7a**	1.52 (0.02) × 10^5	0.0143 (0.0001)	94 (1)
PPARγ/**3a**	1.55 (0.02) × 10^5	0.0190 (0.0001)	123 (2)
PPARα/**7j**	1.01 (0.03) × 10^4	0.0312 (0.0005)	3100 (50)

[a]Experimental error is reported in parentheses.

The affinities of **3a** and **7a** for PPARγ were lower than those of **7j** and Rosi, which is consistent with their low PPARγ transactivation capacity measured in cell-based assays. Remarkably, the partial agonist **7j** shows an affinity for PPARγ similar or higher to that of the full agonist Rosi. It was shown that some compounds with moderate PPARγ agonist activity but with high binding affinity to PPARγ retain significant antidiabetic activity while having fewer and/or less severe adverse events than full PPARγ agonists.[27] Therefore, **7j** can reasonably be considered as the scaffold molecule to develop new antidiabetic drugs.

Specificity. The concentration-dependent activations of PPARδ and PPARα by **3a**, **7a**, and **7j** were analyzed using the appropriate *PPAR-LBD-GAL4* chimera assays. None of the molecules activated PPARδ (Figure S7). Only **7j** transactivated PPARα (Figure 3C and Table 1), with potency between bezafibrate (a weak pan agonist for all three PPAR isoforms) and GW 7647 (a full PPARα agonist). **7j** appeared to be a good PPARα agonist. In order to confirm that **7j** is a PPARα ligand, their direct physical binding was measured by surface plasmon resonance technology-based experiments. We found that **7j** concentration dependently bound to PPARα with a K_d value of 3.1 μM (Table 2).

PPAR forms permissive heterodimers with RXR, thus allowing both the ligands of PPAR and RXR to regulate the transcription of PPAR target genes. Using a mammalian two-hybrid system, we showed that **7j** was less potent and less efficient than Rosi in inducing PPARγ/RXRα heterodimerization (Figure S8A). Moreover, using the *RXRα-LBD-GAL4* chimera assay (Figure S8B) and RXR responsive element (RXRE)-based luciferase assay (Figure S8C), we demonstrated that **7j** is not a direct RXR agonist.

Therefore, **7j** is a dual PPARγ/α agonist (glitazar), and as such, it could theoretically have beneficial synergistic activities on glucose and lipid homeostasis.[19,20]

Binding of 7j, 7a, and 3a to PPARγ. The crystal structure of the complex of PPARγ LBD with the ligand **7j** was solved, collecting diffraction data from apo-crystals soaked for 3 days in the presence of the ligand at 0.5 mM. Initial difference Fourier maps revealed clear electron density for the ligand (Figure S9), showing that it occupies the typical LBD region of the PPARγ agonists (Figure 4A and Figure S10), similar to that of the full agonist Rosi (Figure 4B and Figure S11), with its carboxylate group directly interacting through H bonds with Y473 of helix 12 (H12), at a short distance of 2.3 Å, the two histidines (H323 and H449) of the canonical triad, and S289 (Figure 4A). The NH of the **7j** amide bond is also involved in the H bond with S289, and the CO makes a H bond with Y327. The terminal aliphatic chain of **7j** is in equilibrium between two different conformations (occupation factors of 0.6 and 0.4) and makes vdW contacts with several residues of the internal strand of the β-sheet (Figure 4A and Figure S12) with a consequent effective stabilization of this domain. The isopropyl terminal group of **7j**, makes vdW interactions in the hydrophobic pocket formed by the residues F282, C285, Q286, L453, and L469 (belonging to H3, H11, and H12), contributing, in this way, to a tighter binding of the ligand (Figure 4C and Figure S13).

The thorough analysis of the effective binding network of **7j** into the PPARγ LBD indicates that the ligand is very tightly locked into the LBD, with its carboxylate group strongly interacting with Y473 of H12 (2.3 Å), but in a slightly distorted mode, with respect to Rosi. As a consequence, there is an adjustment of the conformation of helix 12 (H12), the loop 11/12, and the beginning of helix 11 (H11) (Figure 4D and Figure S14). Importantly, H12 is a critical regulatory structural element in the activation function-2 (AF-2) coregulator binding surface, which determines the transcriptional output of PPARγ through differential recruitment of coregulators.

Comparison of the crystal structures of PPARγ in complex with **7j**, **7a**, or **3a**[28] shows no difference in the binding mode of these ligands, regardless of the presence of a carboxylic or hydroxamic head (Figure S15). However, the shorter aliphatic chains of **7a** and **3a** accommodate in a different part of the PPARγ LBD with respect to **7j**, farther away from the β-sheet (Figure S15). Moreover, it is known that partial agonists of PPARγ preferentially stabilize the β-sheet region of the LBD. In the PPARγ/**7j** structure, the long aliphatic chain of the ligand strongly contributes to the stabilization of this region, through vdW interactions, with both its observed conformations facing residues of the innermost β-strand. The solvent entropic gain arising from a more efficacious displacement of water molecules, known to occupy the β-sheet pocket, could

https://dx.doi.org/10.1021/acs.jmedchem.0c01555
J. Med. Chem. XXXX, XXX, XXX−XXX

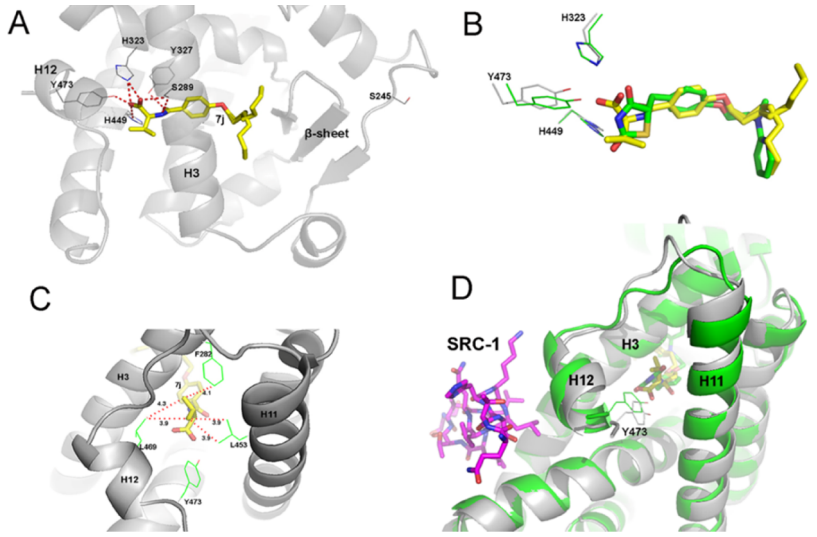

Figure 4. Binding of **7j** to PPARγ. (A) Hydrogen-bond network of **7j** in the PPARγ LBD. (B) Superimposition of **7j** (yellow) and Rosi (green) structures. (C) vdW network of **7j** with residues belonging to H3, H11, and H12 of the PPARγ LBD. (D) Superimposition of **7j** (yellow) and Rosi (green) with the coactivator SRC-1 (magenta); the PPARγ/Rosi structure is colored in green, and the PPARg/**7j** structure is colored in gray (PDB codes: 6QJ5 for PPARγ/**7j** and 2PRG for PPARγ/Rosi).

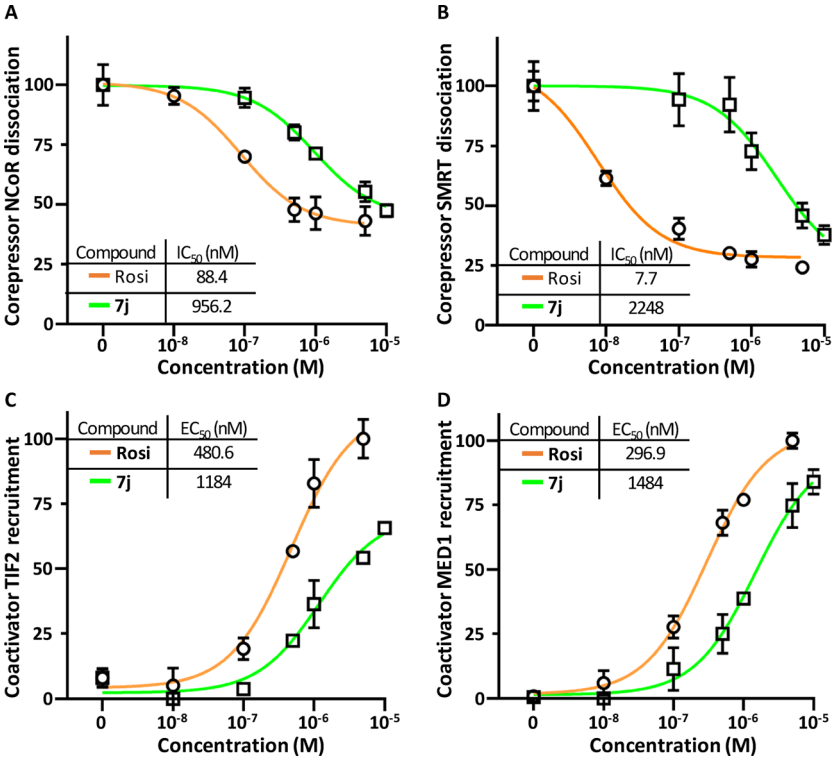

Figure 5. Ligand-specific coregulator binding profiles. (A–D) HEK293 cells were transfected with GAL4-NCoR (A), GAL4-SMRT (B), GAL4-TIF2 (C), GAL4-MED1 (D), and VP16-PPARγ-LBD expression vectors in a mammalian two-hybrid setting and treated with vehicle or various concentrations of **7j** or Rosi. Values are means ± SD expressed as % of the maximal response measured.

play an important role in lowering the free energy of the binding. The higher affinity of **7j** for PPARγ with respect to those of **7a** and **3a** (Table 2) demonstrates that the affinity is largely affected by the length of the aliphatic chain, rather than the character of the acidic head.

Interestingly, a similar unique binding network was observed in the PPARγ crystal structure with the partial agonist SR2067 (Figure S16).[29] Both ligands share a common amide group that forms two hydrogen bonds with Y327 and S289, interactions that are not possible with Rosi. However, unlike **7j**, SR2067 does not interact with Y473.

Interaction of Coregulators with PPARγ. Since Rosi and **7j** stabilize different conformations of the AF2 coregulator binding surface of PPARγ, we analyzed how these molecules modulate the interaction of PPARγ with some of its coregulators. In the mammalian two-hybrid system, **7j** was less potent than Rosi in inducing displacement of the NCoR and SMRT corepressors from PPARγ and in inducing

https://dx.doi.org/10.1021/acs.jmedchem.0c01555
J. Med. Chem. XXXX, XXX, XXX−XXX

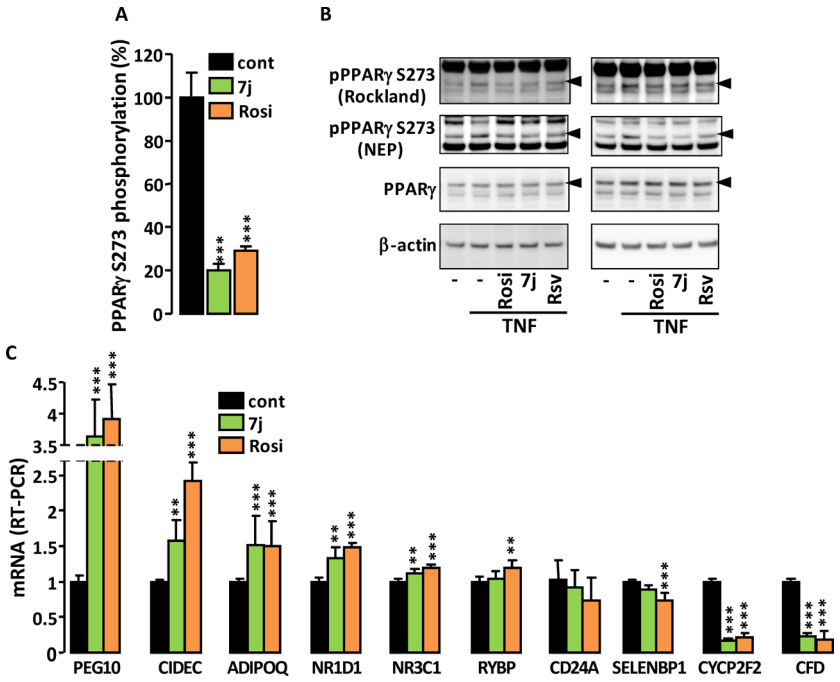

Figure 6. Effect of **7j** on PPARγ phosphorylation. (A) Percentage of *in vitro* PPARγ Ser273 phosphorylation by CDK5 in the presence of 0.1 μM of **7j** or Rosi. (B) Phosphorylation of PPARγ Ser273 in 3T3-L1 adipocyte incubated for 60 min with 5 μM Rosi, **7j**, or roscovitine (Rsv) before TNFα stimulation (50 ng mL^{-1}; 90 min). Two independent experiments are shown. Phosphospecific antibodies were from Rockland or New England Peptide (NEP). Arrow heads indicate phosphorylated PPARγ and PPARγ2. (C) RT-PCR analysis of the expression levels of a selection of genes known to be regulated by CDK5-dependent phosphorylation of PPARγ. Values are means ± SD (n = 5) expressed relative to the mean of control. $^{**}p < 0.01$ and $^{***}p < 0.001$ vs control (one-way ANOVA followed by Dunnett's post-hoc test).

recruitment of TIF2 and MED1 coactivators to PPARγ (Figure 5).

The differences between the profiles of the concentration–response curves of **7j** and Rosi to modulate the interaction of PPARγ with its partners (NCoR, SMRT, TIF2, MED1, mediator, and also RXRα) suggest that these two molecules induce distinct patterns of coregulatory protein recruitment.

CDK5-Mediated Phosphorylation of PPARγ. Part of the antidiabetic effects of PPARγ partial agonists has been associated with their ability to prevent the CDK5-mediated phosphorylation of the PPARγ serine 273 residue.[17,18] Therefore, we assessed the ability of **7j** to inhibit such phosphorylation. An ELISA protocol was optimized to quantify the phosphorylation of PPARγ triggered *in vitro* by recombinant CDK5. **7j** prevented the phosphorylation of PPARγ serine 273 at least as efficiently as Rosi (Figure 6A). Furthermore, pretreatment of 3T3-L1 adipocytes with **7j** or Rosi reduced the TNFα-stimulated phosphorylation of PPARγ serine 273 (Figure 6B). The involvement of CDK5 in this phosphorylation was attested by the fact that it was impeded by treatment of cells with roscovitine, a CDK5 inhibitor. Moreover, out of 10 genes known to be significantly controlled by CDK5-dependent PPARγ phosphorylation in fully differentiated adipocytes,[17,18] seven were regulated in the same way by **7j** and Rosi (Figure 6C). Two genes were only regulated by Rosi, and the expression of one gene was not significantly modified by **7j** and Rosi, although both molecules tended to alter this expression in the same direction.

These results underline the ability of **7j** to reduce CDK5-mediated phosphorylation of PPARγ serine 273 and to alter the expression of genes controlled by PPARγ phosphorylation. This feature supports a potential antidiabetic effect of **7j**.

Adipocyte Differentiation and Glucose Uptake. Adipogenesis-mediated weight gain is a major side effect of PPARγ full agonists.[30] Partial PPARγ agonists are expected to have a reduced effect on lipid storage while maintaining a significant insulin sensitization effect. Therefore, the proadipogenic properties of **3a**, **7a**, and **7j** were compared to that of Rosi. 3T3-L1 fibroblast cells were incubated in the presence of PPARγ agonists as the sole inducer of adipocyte differentiation. Only **7j** and Rosi (the strongest PPARγ agonists) significantly increased the intracellular lipid content (Figure 7A and Figure S17A), showing that these two molecules stimulate adipocyte differentiation. However, for the same concentration, the proadipogenic property of **7j** was significantly lower than that of Rosi. To ascertain that the proadipogenic effect of **7j** involved PPARγ activation, 3T3-L1 cells were coincubated with the specific PPARγ antagonist GW 9662 and with **7j**; then, intracellular lipid accumulation was measured. This approach has been successfully used to demonstrate the involvement of PPARγ activation in the proadipogenic effect of Rosi.[31] Because of its short half-life, GW 9662 was added every day, and to simplify the experiment, the duration of the treatment was reduced to 4 days instead of 6 days, thus limiting the intracellular lipid accumulation. Antagonizing PPARγ activation significantly prevented **7j**- and Rosi-induced adipogenesis (Figure 7B and Figure S17B), showing that PPARγ activation is necessary for the proadipogenic effect of these molecules. When 3T3-L1 fibroblast cells were primed for adipocyte differentiation using the conventional adipogenic cocktail (insulin, dexamethasone, and IBMX) and then treated for 7 days with **3a**, **7a**, **7j** or Rosi, mRNA levels of the markers of adipocyte differentiation were all increased in proportion to the ability of the molecules to activate PPARγ (Figure 7C).

https://dx.doi.org/10.1021/acs.jmedchem.0c01555
J. Med. Chem. XXXX, XXX, XXX−XXX

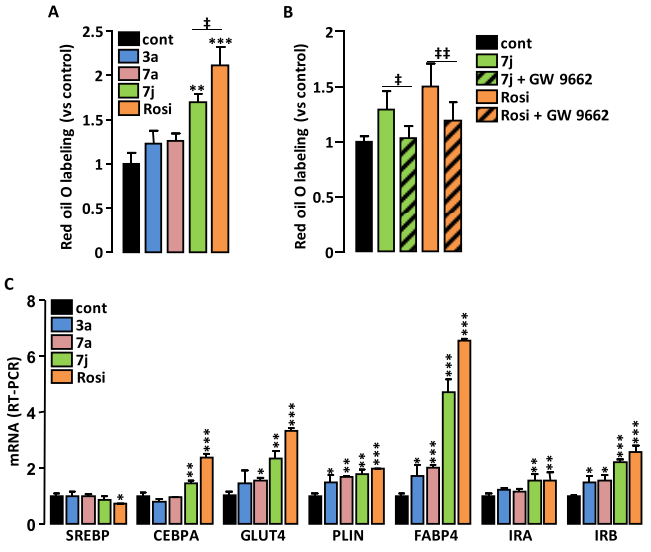

Figure 7. Adipogenic effect of the compounds. (A, B) 3T3-L1 fibroblasts were incubated for 6 days (A) or for 4 days (B) with insulin (350 nM), the indicated PPARγ agonists (1 μM), and the PPARγ antagonist GW 9662 (5 μM). Intracellular lipids were stained with Oil Red O, and then colored lipids were quantified. (C) 3T3-L1 adipocyte differentiation was triggered by the standard mixture of inductors, and then cells were incubated for 7 days with **3a**, **7a**, **7j** (1 μM), or Rosi (0.1 μM). The expression levels of adipogenesis-related genes were measured by RT-PCR. Values are means ± SD expressed as fold relative to untreated situation. $^{*}p < 0.05$, $^{**}p < 0.01$, and $^{***}p < 0.001$ vs control (one-way ANOVA followed by Dunnett's post-hoc test); $^{‡}p < 0.05$ and $^{‡‡}p < 0.01$ (*t*-test).

As expected for partial PPARγ agonists, **3a**, **7a**, and **7j** have reduced proadipogenic properties compared with the full agonist Rosi.

It has been shown that the ability of PPARγ ligands to increase cellular glucose uptake is not necessarily related to their transactivation activity or proadipogenic potential.[32] Therefore, glucose uptake was measured in fully differentiated 3T3-L1 adipocytes after an acute treatment with PPARγ agonists. The insulin-dependent glucose uptake was increased by a short-term treatment with **7j** or Rosi (Figure 8), denoting that part of their insulin sensitizing effect is independent of their ability to increase adipocyte differentiation.

Adipocyte Browning. Brown fat is a target for antiobesity and antidiabetes experimental therapies that aim to increase energy expenditure.[33] Interestingly, strong PPARγ agonists activate the "browning" of white adipose tissues,[34,35]

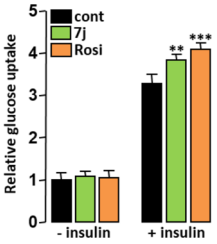

Figure 8. Adipocyte glucose uptake. 3T3-L1 adipocytes were treated with **7j** (1 μM) or Rosi (0.1 μM) for 16 h prior to insulin stimulation (50 nM, 10 min), and cellular glucose uptake was determined. Values are mean ± SD expressed as fold relative to the control situation. $^{**}p < 0.01$ and $^{***}p < 0.001$ vs control (one-way ANOVA followed by Dunnett's post-hoc test).

suggesting that partial PPARγ agonists, which retain significant white fat browning ability, may also have therapeutic benefits in the treatment of obesity and diabetes. We therefore studied the ability of **3a**, **7a**, and **7j** to induce brite/brown-like adipocytes in 3T3-L1 cells.

Only **7j** (and Rosi) upregulated mRNA levels of genes considered as brite/brown adipocyte-selective transcript (Figure 9A,B).[36] Immunoblotting analysis confirmed that **7j** and Rosi increased the expression of uncoupling protein 1 (UCP1), which is a functional marker of brown adipocytes (Figure 9B inset). Coherent with their adipocyte browning effect, Rosi and **7j** increased mRNA levels of additional genes involved in (or associated with) mitochondrial biogenesis (Figure 9C)[37] and in accordance with these two molecules significantly increased the selective labeling of active mitochondria by the MitoTracker dye (Figure 9D). We have previously shown that Rosi induced the conversion of hMADS white adipocytes into brite adipocytes as evidenced by the strong expression of UCP1.[38] In order to test whether compounds **3a**, **7a**, and **7j** were able to substitute for Rosi, hMADS cells first differentiated into white adipocytes were treated with these compounds between days 14 and 18. UCP1 expression was analyzed as an indicator of the degree of white-to-brown adipocyte conversion. UCP1 mRNA levels were increased in **3a**, **7a** and **7j**-treated cells compared to untreated cells, and **7j** was found to be the most potent compound (Figure 9E), although less potent than Rosi (Figure 9F). The PPARγ agonists also increased the levels of UCP1 antigen, which is consistent with observations of its mRNA levels (Figure 9G).

The expression of the adipogenic marker perilipin was not modified by Rosi or **7j** (Figure S18A), whereas the expression of adiponectin, a PPARγ-responsive gene, was more efficiently increased by Rosi than by **7j** (Figure S18B), which confirms that the PPARγ agonist activity of **7j** is lower than that of Rosi.

These data suggest that **7j** can efficiently promote the conversion from white to brown adipocytes.

Lipid Accumulation in Hepatocytes. As PPARα agonists decrease hepatic steatosis,[5,7] we compared the effect of **7j** (dual PPARα/γ agonist) to those of GW 7647 (PPARα agonist) and Rosi (PPARγ agonist) on the lipid accumulation into hepatocytes. In primary rat hepatocytes, only GW 7647 prevented the basal intracellular lipid accumulation and oleic acid-induced lipid accumulation was prevented by Rosi, **7j**, and GW 7647 (Figure 10 A). In human HuH7 hepatoma cells, **7j** and GW 7647 similarly prevented the oleic acid-stimulated lipid accumulation (Figure 10B). These results suggest that **7j** is a promising compound to prevent hepatic steatosis.

Cytotoxicity of 7j. We confirmed, as previously reported,[39−41] that viability, membrane integrity, and apoptosis of primary hepatocytes were not significantly altered by concentrations of Rosi up to 10 μM. These parameters were also not altered by the **7j** compound (Figure S19).

CONCLUSIONS

We have described the synthesis and optimization of compound **7j**: a new *N*-aryl-substituted valine derivative with a balanced agonist activity on PPARα and PPARγ. Compound **7j** occupies the typical LBD region of the PPARγ agonists with a unique high-affinity binding mode and efficiently prevents CDK5-mediated phosphorylation of

https://dx.doi.org/10.1021/acs.jmedchem.0c01555
J. Med. Chem. XXXX, XXX, XXX−XXX

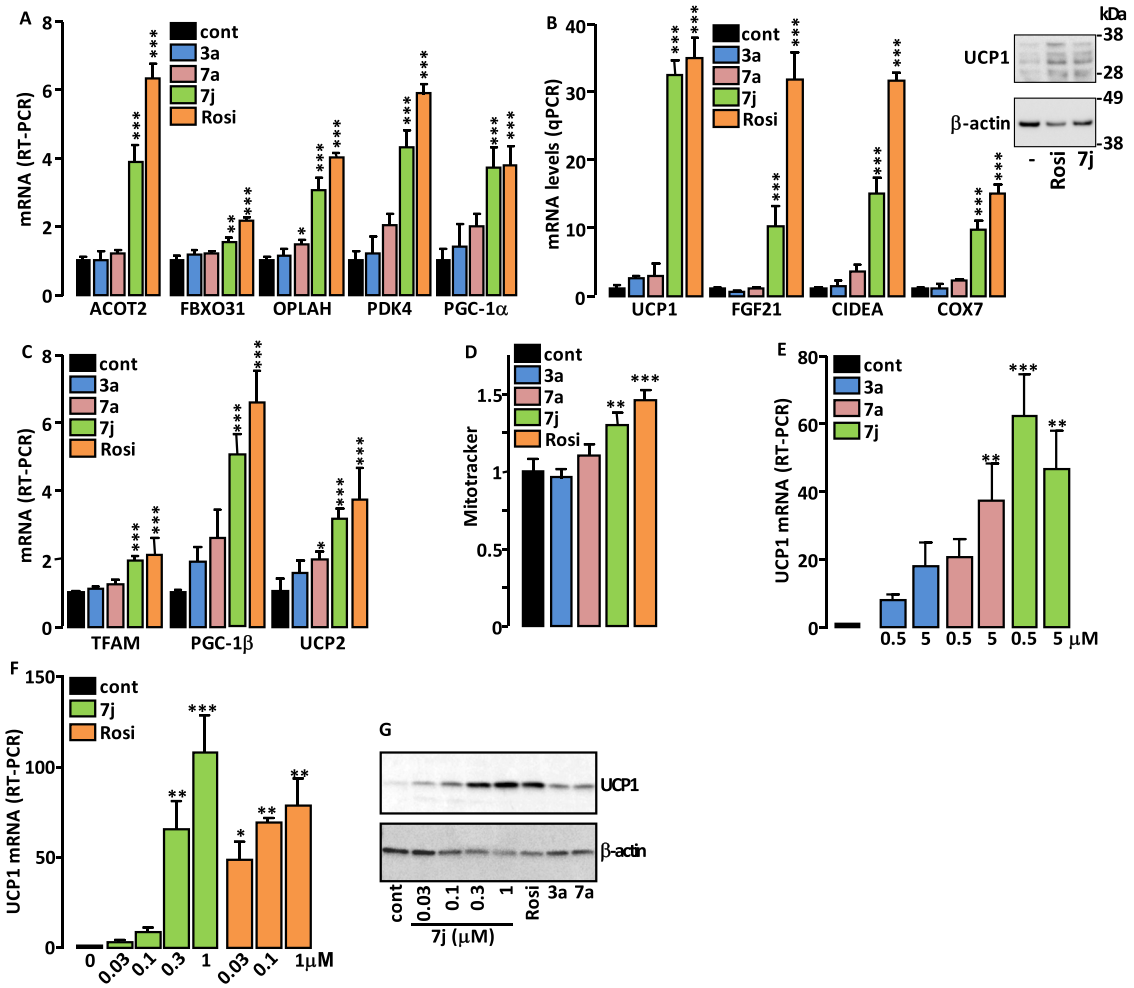

Figure 9. Adipocyte browning effect of the compounds. 3T3-L1 cells were treated as in Figure 7C. (A–C) Expression levels of beige (A) and brown (B) adipocyte markers as well as those of genes involved in mitochondrial biogenesis (C) were measured by RT-PCR. Inset in panel B: immunodetection of UCP1 and β-actin (loading control) in lysates of 3T3-L1 cells treated with **7j** and Rosi. (D) Adipocyte mitochondria content was evaluated by flow cytometry after their selective labeling with MitoTracker dye. (E, F) hMADS white adipocytes were treated with the indicated compounds, and UCP1 mRNA levels were measured by RT-PCR. (G) Immunodetection of UCP1 and β-actin (loading control) in lysates of hMADS treated with the indicated concentrations of **7j**, Rosi (0.1 μM), **3a**, and **7a** (1 μM). Values are mean ± SD expressed as fold relative to the control (cont) situation. *p < 0.05, **p < 0.01, and ***p < 0.001 vs control (one-way ANOVA followed by Dunnett's post-hoc test).

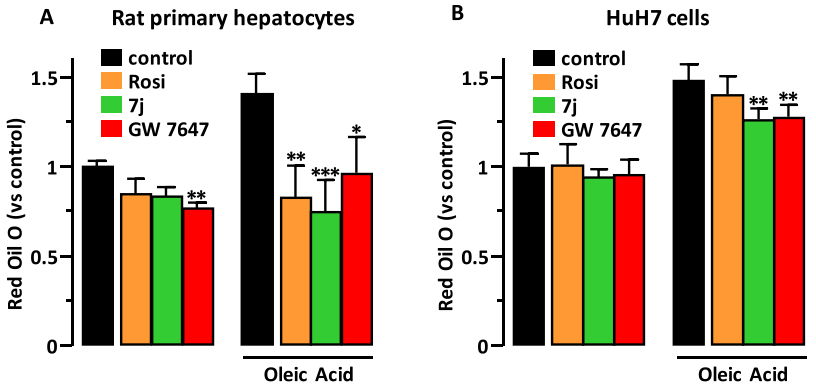

Figure 10. Lipid accumulation in hepatocytes. (A) Primary rat hepatocytes and (B) human HuH7 hepatoma cells were treated with **7j**, Rosi, or GW 7647 (1 μM) for 8 h before addition of oleic acid (0.25 mM). Twenty-four hours later, cellular lipid content was measured by Oil Red O staining. Values are mean ± SD expressed as fold relative to the control. *p < 0.05, **p < 0.01, and ***p < 0.001 vs control (Kruskal–Wallis followed by Dunn's post-hoc test).

PPARγ. Meanwhile, poorly proadipogenic, compound **7j** increases adipocyte insulin-stimulated glucose uptake and efficiently promotes white-to-brown adipocyte conversion. In addition, compound **7j** prevents the oleic acid-induced lipid

https://dx.doi.org/10.1021/acs.jmedchem.0c01555
J. Med. Chem. XXXX, XXX, XXX–XXX

accumulation in hepatocytes. The unique biochemical properties of compound **7j**, its specific biological activities, and its low toxicity make it a promising candidate for the development of compounds to reduce insulin resistance, obesity, and NAFLD.

EXPERIMENTAL SECTION

Chemistry. All solvents were purified according to reported procedures, and reagents were used as commercially available. Methanol, ethyl acetate, dichloromethane, ammonia, and petroleum ether (35−60 °C) were purchased from VWR and used without further purification. Column chromatography was performed on VWR silica gel (70−230 mesh). ^{1}H NMR and ^{13}C NMR spectra were recorded in $CDCl_3$ or DMSO-d_6 on a Bruker AC 300 spectrometer working at 300 and 75 MHz, respectively (the usual abbreviations are used: s, singlet; d, doublet; t, triplet; q, quadruplet; and m, multiplet). Tetramethylsilane was used as the internal standard. All chemical shifts are given in ppm. Purity of all the new compounds evaluated by HPLC (Agilent 1100, C18) analysis was >95%.

Typical Procedure for the Synthesis of Amino Acid Methyl Ester Hydrochloride Derivatives. *Synthesis of L-Valine Methyl Ester Hydrochloride.* In a two-neck round flask equipped with a condenser was placed at room temperature 3 g of L-valine (2.56×10^{-2} mol) in 20 mL of methanol. The mixture was placed under stirring at 0 °C, and 3.4 mL of thionyl chloride (4.7×10^{-3} mol) was slowly added. After removal of the solvents, diethyl ether was added and the product precipitates as a white solid. After filtration, the product was dried under vacuum to afford the expected L-valine methyl ester hydrochloride in 86% yield.

White solid. ^{1}H NMR (D_2O): δ = 4.14−4.17 (m, 1H), 3.80−3.85 (m, 3H), 2.50−2.56 (m, 1H), 1.12−1.15 (m, 6H). ^{13}C NMR (D_2O): δ = 168.91, 58.57, 53.02, 29.95, 18.15.

*(S)-2-(4-Hexyloxy-benzoylamino)-3-methyl-butyric Acid Methyl Ester (**6**).* In a two-neck round flask equipped with a condenser were placed at room temperature 2.34 g of benzotriazol-1-yloxytris-(dimethylamino)phosphonium hexafluorophosphate (BOP; 5.26×10^{-3} mol), 2.34 mL of diisopropylethylamine (1.8×10^{-2} mol), 1.2 g of 4-(hexyloxy)benzoic acid (5.40×10^{-3} mol), and 0.88 g of L-valine methyl ester hydrochloride (5.25×10^{-3} mol) in 15 mL of CH_2Cl_2. The mixture was placed under stirring at room temperature for 24 h. Water was added to allow phase separation. The bottom phase layer was washed with $NaHCO_3$ (10%) solution, dried over Na_2SO_4, filtered, and concentrated in vacuo. After removal of the solvents, the crude residue was purified by chromatography on a silica gel column using CH_2Cl_2/ethyl acetate (1/1) as the eluent, affording the expected product **6** in 85% yield.

White solid. ^{1}H NMR ($CDCl_3$): δ = 8.06 (m, 2H), 7.15 (m, 2H), 4.15−4.22 (m, 4H), 3.71−3.75 (m, 3H), 1.81−2.05 (m, 3H), 1.21−1.37 (m, 6H), 0.69−0.92 (m, 9H). ^{13}C NMR ($CDCl_3$): δ = 172.90, 166.54, 160.52, 133.08, 130.21, 130.01, 114.55, 68.22, 57.56, 52.34, 33.49, 31.32, 29.34, 25.67, 22.61, 18.48, 14.03. MS (ESI) *m/z*: calcd for $C_{19}H_{29}NO_4$, 336.2146 (100%, (M + H$^+$)).

*4-Hexyloxy-N-((S)-1-hydroxycarbamoyl-2-methyl-propyl)-benzamide (**3a**).* In a 25 mL round flask was placed at room temperature 0.6 g of **6** (1.78×10^{-3} mol) in 15 mL of ethanol. A hydroxylamine solution (40%, 2 mL) was subsequently added, and the mixture was allowed to stir at reflux for 24 h. After removal of the solvents, the crude residue was purified by chromatography on a silica gel column using petroleum ether/ethyl acetate (1/1) and methanol/ethyl acetate (1/1) as eluents, affording the expected product **3a** in 72% yield.

White solid. ^{1}H NMR (DMSO-d_6): δ = 8.01 (m, 2H), 7.09 (m, 2H), 3.95−3.98 (m, 3H), 1.78−1.82 (m, 2H), 1.01−1.31 (m, 6H), 0.71−0.93 (m, 9H). ^{13}C NMR (DMSO-d_6): δ = 167.20, 166.23, 161.1, 133.41, 129.80, 113.98, 69.41, 57.31, 31.03, 29.42, 25.76, 22.43, 18.62, 13.89. MS (ESI) *m/z*: calcd for $C_{18}H_{28}N_2O_4$, 337.2045 (100%, (M + H$^+$)).

*4-Hexyloxy-N-[(S)-1-hydroxycarbamoyl-2-(3H-imidazol-4-yl)-ethyl]-benzamide (**3b**).* The procedure is similar to that applied for the preparation of **3a.**

Pale yellow solid. ^{1}H NMR (DMSO-d_6): δ = 7.52−7.89 (m, 3H), 6.89−7.42 (m, 5H), 5.55 (s, 2H), 4.75−4.73 (m, 2H), 4.10−4.19 (m, 2H), 1.22−1.92 (m, 9H), 0.89−0.96 (m, 3H). ^{13}C NMR (DMSO-d_6): δ = 174.19, 164.07, 162.03, 133.17, 129.03, 123.47, 118.22, 115.35, 67.56, 52.96, 30.99, 30.91, 29.05, 25.49, 22.54, 14.25. MS (ESI) *m/z*: calcd for $C_{19}H_{26}N_4O_4$, 375.2014 (100%, (M + H$^+$)).

*4-Hexyloxy-N-[(S)-1-hydroxycarbamoyl-2-(1H-indol-2-yl)-ethyl]-benzamide (**3c**).* The procedure is similar to that applied for the preparation of **3a.**

White solid. ^{1}H NMR (DMSO-d_6): δ = 7.32−7.62 (m, 5H), 6.29−7.25 (m, 7H), 3.92−4.03 (m, 2H), 2.89−3.34 (m, 4H), 1.20−1.79 (m, 6H), 0.88−0.92 (m, 3H). ^{13}C NMR (DMSO-d_6): δ = 172.22, 168.98, 161.25, 139.48, 131.05, 129.14, 126.29, 120.15, 118.78, 113.69, 110.36, 104.25, 71.24, 53.32, 30.21, 28.28, 25.14, 22.04, 14.13. MS (ESI) *m/z*: calcd for $C_{24}H_{29}N_3O_4$, 424.2236 (100%, (M + H$^+$)).

*4-Hexyloxy-N-((S)-2-hydroxy-1-hydroxycarbamoyl-ethyl)-benzamide (**3d**).* The procedure is similar to that applied for the preparation of **3a.**

White solid. ^{1}H NMR (DMSO-d_6): δ = 7.02−7.51 (m, 4H), 3.62−4.20 (m, 5H), 1.31−1.82 (m, 9H), 0.89−0.92 (m, 3H). ^{13}C NMR (DMSO-d_6): δ = 170.36, 168.24, 160.89, 130.14, 125.34, 113.47, 68.78, 61.24, 53.89, 31.01, 28.14, 25.98, 21.33, 13.88. MS (ESI) *m/z*: calcd for $C_{16}H_{24}N_2O_5$, 325.1768 (100%, (M + H$^+$)).

*4-Hexyloxy-N-((S)-1-hydroxycarbamoyl-2-phenyl-ethyl)-benzamide (**3e**).* The procedure is similar to that applied for the preparation of **3a.**

White solid. ^{1}H NMR (DMSO-d_6): δ = 7.66−7.68 (m, 2H), 6.47−7.16 (m, 2H), 3.55−3.97 (m, 2H), 2.89−3.23 (m, 2H), 1.35−1.74 (m, 8H), 0.90−0.91 (m, 3H). ^{13}C NMR (DMSO-d_6): δ = 178.45, 168.32, 161.25, 137.47, 129.02, 125.68, 114.98, 60.01, 53.87, 40.36, 30.23, 28.14, 24.12, 22.98, 13.48. MS (ESI) *m/z*: calcd for $C_{22}H_{28}N_2O_4$, 385.2057 (100%, (M + H$^+$)).

*N-[(S)-2-(3,4-Dihydroxy-phenyl)-1-hydroxycarbamoyl-ethyl]-4-hexyloxy-benzamide (**3f**).* The procedure is similar to that applied for the preparation of **3a.**

White solid. ^{1}H NMR (DMSO-d_6): δ = 7.71−7.73 (m, 2H), 6.59−6.93 (m, 4H), 6.32 (s, 1H), 5.87 (s, 1H), 3.99−4.02 (m, 2H), 2.95−2.99 (m, 2H), 1.17−2.02 (m, 9H), 0.87−0.89 (m, 3H). ^{13}C NMR (DMSO-d_6): δ = 171.25, 168.33, 160.58, 146.01, 143.69, 128.69, 126.47, 123.74, 116.36, 115.47, 69.71, 52.34, 38.38, 28.47, 22.14, 25.69, 22.47, 13.12. MS (ESI) *m/z*: calcd for $C_{22}H_{28}N_2O_6$, 417.1934 (100%, (M + H$^+$)).

*4-Hexyloxy-N-((S)-1-hydroxycarbamoyl-4-methylsulfanyl-butyl)-benzamide (**3g**).* The procedure is similar to that applied for the preparation of **3a.**

White solid. ^{1}H NMR (DMSO-d_6): δ = 6.91−7.69 (m, 5H), 1.17−2.74 (m, 20H), 0.87−0.88 (m, 3H). ^{13}C NMR (DMSO-d_6): δ = 170.78, 168.65, 162.21, 128.12, 125.14, 117.77, 69.66, 51.45, 34.12, 31.78, 28.02, 25.63, 22.33, 15.15, 13.19. MS (ESI) *m/z*: calcd for $C_{19}H_{30}N_2O_4S$, 383.1935 (100%, (M + H$^+$)).

*4-(Hexyloxy)-N-((2S,3S)-3-hydroxy-1-(hydroxyamino)-1-oxobutan-2-yl)benzamide (**3h**).* The procedure is similar to that applied for the preparation of **3a.**

White solid. ^{1}H NMR (DMSO-d_6): δ = 7.71−7.73 (m, 2H), 6.98−7.11 (m, 3H), 5.32 (s, 1H), 4.60−4.65 (m, 1H), 4.06−4.44 (m, 3H), 1.80−1.92 (m, 1H), 1.07−1.37 (m, 12H). ^{13}C NMR (DMSO-d_6): δ = 169.75, 167.63, 162.54, 132.53, 125.82, 114.51, 68.78, 67.63, 59.34, 31.88, 28.02, 24.89, 22.33, 15.12, 13.89. MS (ESI) *m/z*: calcd for $C_{17}H_{26}N_2O_5$, 339.1879 (100%, (M + H$^+$)).

*(S)-N-(1-(Hydroxyamino)-3-methyl-1-oxobutan-2-yl)-4-methoxybenzamide (**4a**).* White solid. ^{1}H NMR (DMSO-d_6): δ = 0.91−0.96 (m, 6H), 2.16−2.23 (m, 1H), 3.84 (s, 3H), 4.33−4.45 (m, 1H), 6.98−7.53 (m, 2H), 7.83−7.89 (m, 2H), 8.79 (s, 2H). ^{13}C NMR (DMSO-d_6): δ = 174.44, 170.42, 164.51, 130.95, 127.71, 115.17, 56.40, 52.96, 32.19, 20.12, 19.65. MS (ESI) *m/z*: calcd for $C_{13}H_{18}N_2O_4$, 267.1386 (100%, (M + H$^+$)).

https://dx.doi.org/10.1021/acs.jmedchem.0c01555
J. Med. Chem. XXXX, XXX, XXX−XXX

*(S)-4-Ethoxy-N-(1-(hydroxyamino)-3-methyl-1-oxobutan-2-yl)-benzamide (**4b**).* White solid. ^{1}H NMR (DMSO-d_6): δ = 0.91−0.95 (m, 6H), 1.49 (t, J = 7.0 Hz, 3H), 1.68−1.75 (m, 1H), 4.01−4.11 (m, 2H), 4.31−4.41 (m, 1H), 6.94−6.99 (m, 2H), 7.80−7.85 (m, 2H), 8.59 (s, 2H). ^{13}C NMR (DMSO-d_6): δ = 171.10, 166.47, 166.91, 132.01, 129.30, 114.59, 63.42, 56.95, 30.10, 18.64, 14.69. MS (ESI) m/z: calcd for $C_{14}H_{20}N_2O_4$, 281.1412 (100%, (M + H$^+$)).

*(S)-N-(1-(Hydroxyamino)-3-methyl-1-oxobutan-2-yl)-4-propoxy-benzamide (**4c**).* White solid. ^{1}H NMR (DMSO-d_6): δ = 0.92−1.12 (m, 9H), 1.69−1.89 (m, 2H), 3.27−3.38 (m, 2H), 3.90−4.02 (m, 2H), 6.90−7.07 (m, 2H), 7.76−7.89 (m, 2H). ^{13}C NMR (DMSO-d_6): δ = 171.14, 165.95, 162.22, 130.95, 128.03, 115.09, 70.35, 57.03, 30.75, 22.63, 18.64, 10.63. MS (ESI) m/z: calcd for $C_{15}H_{22}N_2O_4$, 294.1634 (100%, (M + H$^+$)).

*(S)-4-Butoxy-N-(1-(hydroxyamino)-3-methyl-1-oxobutan-2-yl)-benzamide (**4d**).* White solid. ^{1}H NMR (DMSO-d_6): δ = 0.90−0.98 (m, 9H), 1.52−1.62 (m, 2H), 1.77−1.83 (m, 2H), 2.16−2.22 (m, 2H), 3.97−4.02 (m, 2H), 4.37−4.42 (m, 1H), 7.75−7.77 (m, 2H), 7.98−8.02 (m, 2H), 8.53 (m, 1H). ^{13}C NMR (DMSO-d_6): δ = 171.49, 166.14, 166.16, 133.37, 130.18, 122.86, 69.16, 57.04, 30.74, 30.69, 18.48, 13.75. MS (ESI) m/z: calcd for $C_{16}H_{24}N_2O_4$, 309.1701 (100%, (M + H$^+$)).

*(S)-N-(1-(Hydroxyamino)-3-methyl-1-oxobutan-2-yl)-4-(pentyloxy)benzamide (**4e**).* White solid. ^{1}H NMR (DMSO-d_6): δ = 0.90−0.98 (m, 9H), 1.52−1.62 (m, 2H), 1.77−1.83 (m, 2H), 2.16−2.22 (m, 2H), 3.97−4.02 (m, 2H), 4.37−4.42 (m, 1H), 7.75−7.77 (m, 2H), 7.98−8.02 (m, 2H), 8.53 (m, 1H). ^{13}C NMR (DMSO-d_6): δ = 169.71, 167.51, 162.83, 132.86, 126.86, 119.98, 68.72, 58.13, 31.14, 30.98, 29.34, 28.14, 18.54, 14.16. MS (ESI) m/z: calcd for $C_{17}H_{26}N_2O_4$, 323.1934 (100%, (M + H$^+$)).

*(S)-4-(Heptyloxy)-N-(1-(hydroxyamino)-3-methyl-1-oxobutan-2-yl)benzamide (**4f**).* White solid. ^{1}H NMR (DMSO-d_6): δ = 0.90−0.96 (m, 9H), 1.28−1.74 (m, 10H), 2.02−2.16 (m, 1H), 3.97−4.07 (m, 2H), 4.37−4.42 (m, 1H), 7.03−7.08 (m, 2H), 8.02−8.09 (m, 2H), 8.53 (m, 1H). ^{13}C NMR (DMSO-d_6): δ = 171.09, 166.42, 162.02, 130.07, 129.03, 115.18, 68.15, 57.63, 31.80, 29.18, 26.04, 22.14, 18.74, 13.98. MS (ESI) m/z: calcd for $C_{19}H_{30}N_2O_4$, 351.2245 (100%, (M + H$^+$)).

*(S)-N-(1-(Hydroxyamino)-3-methyl-1-oxobutan-2-yl)-4-(octyloxy)benzamide (**4g**).* White solid. ^{1}H NMR (DMSO-d_6): δ = 0.90−0.97 (m, 9H), 1.29−1.82 (m, 12H), 2.06−2.15 (m, 1H), 3.95−4.07 (m, 2H), 4.32−4.41 (m, 1H), 7.00−7.08 (m, 2H), 8.01−8.10 (m, 2H), 8.51 (m, 1H). ^{13}C NMR (DMSO-d_6): δ = 171.10, 166.35, 162.35, 131.37, 129.90, 115.11, 68.24, 57.52, 31.79, 30.95, 29.31, 26.82, 22.47, 18.63, 14.21. MS (ESI) m/z: calcd for $C_{20}H_{32}N_2O_4$, 365.2423 (100%, (M + H$^+$)).

*(S)-2-(4-Hexyloxy-benzoylamino)-3-methyl-butyric Acid (**7a**).* In a 25 mL round flask was placed at room temperature 0.6 g of **6** (1.78 × 10^{-3} mol) in 15 mL of ethanol. A sodium hydroxide solution (10%, 2 mL) was subsequently added, and the mixture was allowed to stir at room temperature for 24 h. The bottom phase layer was discarded, and the aqueous phase was acidified with HCl (1 N). After extraction with ethyl acetate, the organic phase was dried over Na_2SO_4, filtered, and concentrated in vacuo. The crude residue was purified by chromatography on a silica gel column using petroleum ether/ethyl acetate (1/1) as the eluent, affording the expected product **7a** in 69% yield.

White solid. 1H NMR ($CDCl_3$): δ = 7.80−7.84 (m, 2H), 6.95−7.04 (m, 2H), 4.44−4.46 (m, 1H), 4.02−4.05 (m, 2H), 2.19−2.35 (m, 1H), 1.73−1.84 (m, 2H), 1.43−1.57 (m, 2H), 1.26−1.35 (m, 5H), 1.04 (s, 3H), 1.03 (s, 3H), 0.91−0.94 (m, 3H). ^{13}C NMR ($CDCl_3$): δ = 174.59, 168.63, 162.17, 128.97, 125.94, 113.84, 67.86, 58.88, 31.35, 30.54, 28.87, 25.42, 22.27, 18.43, 17.52, 12.98. MS (ESI) m/z: calcd for $C_{18}H_{27}NO_4$, 322.1932 (100%, (M + H$^+$)).

*(R)-2-(4-Hexyloxy-benzoylamino)-3-methyl-butyric Acid (**7a'**).* The procedure is similar to that applied for the preparation of **7a.**

White solid. ^{1}H NMR ($CDCl_3$): δ = 6.55−7.19 (m, 4H), 3.89−3.99 (m, 3H), 1.50−2.11 (m, 7H), 0.89−1.32 (m, 11H). ^{13}C NMR ($CDCl_3$): δ = 177.56, 166.34, 159.95, 132.36, 130.12, 114.08, 72.30, 64.36, 31.32, 31.04, 29.14, 25.31, 22.14, 18.47, 13.96. MS (ESI) m/z: calcd for $C_{18}H_{27}NO_4$, 322.1932 (100%, (M + H$^+$)).

*(S)-2-(4-Hexyloxy-benzoylamino)-3-phenyl-propionic Acid (**7b**).* The procedure is similar to that applied for the preparation of **7a.**

White solid. ^{1}H NMR ($CDCl_3$): δ = 10.98 (s, 1H), 7.89−8.01 (m, 2H), 6.95−7.21 (m, 7H), 4.83−4.85 (m, 11H), 3.89−3.92 (m, 2H), 3.01−3.03 (m, 2H), 0.95−1.61 (m, 12H). ^{13}C NMR ($CDCl_3$): δ = 176.15, 168.13, 161.14, 140.03, 129.18, 128.82, 123.52, 123.42, 115.22, 73.34, 61.56, 38.78, 33.14, 31.42, 26.14. MS (ESI) m/z: calcd for $C_{23}H_{30}NO_4$, 385.2221 (100%, (M + H$^+$)).

*(S)-2-(4-Hexyloxy-benzoylamino)-3-(3H-imidazol-4-yl)-propionic Acid (**7c**).* The procedure is similar to that applied for the preparation of **7a.**

Yellow solid. ^{1}H NMR ($CDCl_3$): δ = 7.93 (s, 1H), 7.63−7.65 (m, 2H), 6.75−6.92 (m, 4H), 4.69−4.72 (m, 2H), 4.12−3.92 (m, 2H), 2.67−2.78 (m, 2H), 0.76−1.52 (m, 11H). ^{13}C NMR ($CDCl_3$): δ = 174.75, 169.70, 161.08, 132.04, 131.03, 129.92, 125.75, 121.56, 111.04, 68.13, 52.67, 31.14, 29.57, 29.15, 25.56, 22.59, 13.82. MS (ESI) m/z: calcd for $C_{19}H_{25}N_3O_4$, 360.1834 (100%, (M + H$^+$)).

*(S)-2-(4-Hexyloxy-benzoylamino)-3-hydroxy-propionic Acid (**7d**).* The procedure is similar to that applied for the preparation of **7a.**

White solid. ^{1}H NMR (DMSO-d_6): δ = 7.68 (s, 2H), 6.92−6.96 (m, 2H), 3.92−4.54 (m, 6H), 1.20−1.95 (m, 9H), 0.89−0.92 (m, 3H). ^{13}C NMR (DMSO-d_6): δ = 173.32, 166.74, 161.44, 128.45, 125.18, 111.14, 68.84, 62.30, 56.14, 31.12, 29.11, 24.13, 22.59, 14.13. MS (ESI) m/z: calcd for $C_{16}H_{23}NO_5$, 310.1667 (100%, (M + H$^+$)).

*(4-Hexyloxy-benzoylamino)-acetic Acid (**7e**).* The procedure is similar to that applied for the preparation of **7a.**

White solid. ^{1}H NMR (DMSO-d_6): δ = 7.68 (s, 2H), 6.98 (s, 2H), 4.10−4.12 (m, 2H), 3.78 (m, 2H), 1.49−1.76 (m, 8H), 0.89−0.92 (m, 3H). ^{13}C NMR (DMSO-d_6): δ = 172.31, 168.28, 161.02, 130.06, 114.55, 114.53, 66.42, 42.85, 34.56, 32.12, 29.14, 23.12, 21.45, 14.14. MS (ESI) m/z: calcd for $C_{15}H_{21}NO_4$, 280.1511 (100%, (M + H$^+$)).

*(S)-2-(4-Methoxy-benzoylamino)-3-methyl-butyric Acid (**7f**).* The procedure is similar to that applied for the preparation of **7a.**

White solid. ^{1}H NMR (DMSO-d_6): δ = 7.53−7.55 (m, 2H), 6.95−6.97 (m, 2H), 6.05 (s, 1H), 4.75−4.77 (m, 1H), 3.72 (s, 3H), 1.75−1.87 (m, 1H), 1.04−1.06 (m, 6H). ^{13}C NMR (DMSO-d_6): δ = 172.33, 167.28, 160.14, 131.12, 127.30, 110.15, 58.66, 55.65, 30.93, 19.03. MS (ESI) m/z: calcd for $C_{13}H_{17}NO_4$, 251.1232 (100%, (M + H$^+$)).

*(S)-2-(4-Ethoxy-benzoylamino)-3-methyl-butyric Acid (**7g**).* The procedure is similar to that applied for the preparation of **7a.**

White solid. ^{1}H NMR (DMSO-d_6): δ = 7.59 (s, 2H), 7.02−7.05 (m, 2H), 4.16−4.40 (m, 3H), 1.87−1.92 (m, 1H), 1.32−1.36 (m, 3H), 0.98−1.03 (m, 6H). ^{13}C NMR (DMSO-d_6): δ = 173.15, 167.10, 160.83, 129.98, 127.04, 113.21, 61.89, 57.93, 29.98, 19.19, 14.31. MS (ESI) m/z: calcd for $C_{14}H_{19}NO_4$, 266.1342 (100%, (M + H$^+$)).

*(S)-3-Methyl-2-(4-propoxy-benzoylamino)-butyric Acid (**7h**).* The procedure is similar to that applied for the preparation of **7a.**

White solid. ^{1}H NMR (DMSO-d_6): δ = 6.95−7.32 (m, 4H), 6.75 (s, 1H), 3.98−4.05 (m, 3H), 1.54−1.89 (m, 3H), 1.12−1.17 (m, 3H), 0.97−1.02 (m, 6H). ^{13}C NMR (DMSO-d_6): δ = 172.34, 167.42, 160.15, 128.64, 127.42, 112.45, 69.37, 58.62, 29.89, 21.12, 18.82, 10.29. MS (ESI) m/z: calcd for $C_{15}H_{21}NO_4$, 280.1534 (100%, (M + H$^+$)).

*(4-(Heptyloxy)benzoyl)-L-valine (**7i**).* White solid. ^{1}H NMR (DMSO-d_6): δ = 0.93−1.41 (m, 19H), 1.41−1.46 (m, 2H), 2.23−2.35 (m, 1H), 3.87−3.92 (t, J = 5 Hz, 2H), 4.46−4.69 (m, 1H), 6.82−6.89 (m, 2H), 7.66−7.69 (m, 2H). ^{13}C NMR (DMSO-d_6): δ = 175.24, 167.12, 162.78, 129.02, 114.39, 68.28, 57.84, 31.80, 31.27, 29.14, 29.07, 25.98, 22.64, 19.15, 17.92, 14.12. MS (ESI) m/z: calcd for $C_{19}H_{29}NO_4$, 336.2165 (100%, (M + H$^+$)).

*(4-(Octyloxy)benzoyl)-L-valine (**7j**).* White solid. ^{1}H NMR (DMSO-d_6): δ = 0.91−1.34 (m, 10H), 1.38−1.54 (m, 11H), 1.76−1.87 (m, 2H), 2.23−2.37 (m, 1H), 4.0.3−4.08 (t, J = 5 Hz, 2H), 4.48−4.52 (dd, J = 5 Hz, 1H), 6.98−7.01 (m, 2H), 7.83−8.86 (m, 2H). ^{13}C NMR (DMSO-d_6): δ = 175.31, 170.16, 163.59, 130.46,

https://dx.doi.org/10.1021/acs.jmedchem.0c01555
J. Med. Chem. XXXX, XXX, XXX−XXX

127.28, 115.21, 69.24, 59.88, 33.04, 31.82, 30.53, 30.46, 30.34, 27.19, 23.77, 19.79, 18.97, 14.49. MS (ESI) *m/z*: calcd for $C_{20}H_{31}NO_4$, 350.2315 (100%, (M + H^+)).

(4-(Decyloxy)benzoyl)-L-valine (7k). White solid. ^{1}H NMR (DMSO-d_6): δ = 0.92−1.32 (m, 10H), 1.44−1.54 (m, 15H), 1.82−1.88 (m, 2H), 2.33−2.46 (m, 1H), 3.94−4.06 (m, 2H), 4.82−4.87 (m, 1H), 6.86−6.94 (m, 2H), 7.73−7.83 (m, 2H) ^{13}C NMR (DMSO-d_6): δ = 175.36, 167.71, 162.20, 129.31, 129.10, 125.71, 114.33, 114.15, 68.25, 57.62, 31.94, 31.43, 29.61, 29.43, 29.37, 29.16, 26.03, 22.73, 19.09, 17.91, 14.18. MS (ESI) *m/z*: calcd for $C_{22}H_{35}NO_4$, 378.2645 (100%, (M + H^+)).

Chemicals. Rosiglitazone, bezafibrate, and roscovitine were from Sigma-Aldrich (Saint-Quentin-Fallavier, France). GW 7647 was from Axon Medchem (Groningen, The Netherlands). GW 9662 and SR 11235 were from Santa Cruz Biotechnology (Santa Cruz, CA, USA).

Antibodies. PPARγ antibody (E-8) was from Santa Cruz Biotechnology. PPARγ phospho Ser273 antibodies were from Rockland (Limerick, PA, USA) or custom produced by New England Peptide (Gardner, MA, USA). UCP1 antibodies (ab10983) were from Abcam (Cambridge, MA, USA). β-actin (13E5) was from Cell Signaling Technology (Danvers, MA, USA).

Cell Culture. Media and cell culture reagents were from Thermo Fisher Scientific (Illkirch-Graffenstaden, France). HEK293 cells (GripTite 293 MSR) were from Thermo Fisher Scientific. 3T3-L1 cells (from ATCC) were routinely cultured in DMEM with 4 mM L-glutamine, 4.5 g L^{-1} glucose, and 0.11 g L^{-1} sodium pyruvate and supplemented with 10% fetal bovine serum and antibiotics. Two days after confluence, adipocyte differentiation was triggered by changing the conventional induction mixture (0.1 μM dexamethasone, 500 μM 3-isobutyl-1-methylxanthine, and 174.5 nM insulin from Sigma-Aldrich, L'Isle d'Abeau Chesnes, France). After 48 h, the medium was removed and replaced by a fresh medium containing only 174.5 nM insulin. HuH7 hepatoma cells from the Japanese Cancer Research Resources Bank were cultured in DMEM containing 10% fetal bovine serum (FBS). At the confluence, cells were treated for 24 h with 0.25 mM oleic acid (Sigma-Aldrich) complexed with BSA. The establishment, characterization, and culture protocols of human multipotent adipose-derived stem (hMADS) cells have been described previously.[42] Briefly, confluent cells were submitted to differentiation medium (DMEM/Ham's F12 media containing 10 μg mL^{-1} transferrin, 10 nM insulin, and 0.2 nM triiodothyronine from Sigma-Aldrich) supplemented with 1 μM dexamethasone and 500 μM isobutyl-methylxanthine. Two days later, the medium was changed, dexamethasone and isobutyl-methylxanthine were omitted, and 100 nM Rosi (Sigma-Aldrich) was added for the indicated periods. Cells were treated between days 2 and 9 with Rosi to enable white adipocyte differentiation to take place. After 5 days in the absence of Rosi, brite adipocyte conversion was induced by adding compounds to be tested (day 14). The medium was changed every other day, and cells were used at day 18. Pooled plateable cryopreserved primary rat hepatocytes (Male, Sprague−Dawley) from XenoTech (Kansas city, KS, USA) were plated and cultured as described by the manufacturer.

Cell Viability, Toxicity, and Apoptosis Assay. Cell viability was monitored using the CellTiter-Blue cell viability assay (Promega, Madison, WI) based on the ability of living cells to convert resazurin into the fluorescent end product resorufin and by measuring cellular ATP levels, which decline rapidly when cells undergo necrosis or apoptosis, using an ATPLite 1step luminescence assay system (PerkinElmer, Waltham, MA, USA) according to the manufacturer's instructions. Cytotoxicity was determined by measuring the lactate dehydrogenase (LDH) released into the culture medium upon plasma membrane damage using the LDH-Glo cytotoxicity assay (Promega). Apoptosis was determined by measuring caspase 3/7-dependent cleavage of a luminogenic substrate using the Caspase-Glo 3/7 Assay (Promega). Experiments were performed two to three times in triplicate.

Cellular Lipid Content Staining and Measurement. *Oil Red O staining.* 3T3-L1 cells, HuH7 hepatoma cells, or primary rat hepatocytes were washed with PBS and fixed with 4% formaldehyde solution for 20 min, then washed again, and stained with 0.35% Oil Red O solution (Sigma-Aldrich) in 60% isopropanol for 20 min. Then, cells were washed with water, and photographs were taken. The stain from the cells was eluted using 100% isopropanol, and the absorbance of the eluted stain was read at 490 nm. Experiments were performed five times in duplicate for cell lines and twice in triplicate for primary cells.

AdipoRed assay. 3T3-L1 preadipocytes were cultured in a black 96-well plate. Two days post-confluency, cells were incubated with the test molecules (10 μM) for 7 additional days. Cells were washed with PBS, and then a solution of AdipoRed reagent (1/40 in PBS) was added into each well. After 10 min at room temperature and in the dark, fluorescence was measured at 485 and 572 nm for excitation and emission, respectively, on an EnSight microplate reader (PerkinElmer) in the scanning mode. Since this technique was used for screening purposes, the experiment was performed once in duplicate.

2-Deoxy-D-glucose Uptake Assay. Glucose uptake activity of fully differentiated 3T3-L1 adipocytes was measured by the chemiluminescent assay[43] using a Glucofax kit as described by the manufacturer (Yelen, Ensues la Redonne, France). Briefly, 3T3-L1 adipocytes (80% of the cells displaying the characteristic lipid-filled phenotype) were gently detached from the plate by Accutase (Thermo Fisher Scientific) treatment, seeded (3.5×10^4 cells $well^{-1}$) at confluence in 96-well culture dishes, and cultured for 2 more days in DMEM supplemented with 10% FBS. Adipocytes were then incubated in glucose-free DMEM for 4 h, then washed twice with Krebs-Ringer-phosphate-Hepes (KRPH) buffer (20 mM Hepes, 5 mM KH_2PO_4, 1 mM $MgSO_4$, 1 mM $CaCl_2$, 136 mM NaCl, and 4.7 mM KCl at pH 7.4) containing 0.2% BSA, and incubated 30 min in 100 μL of KRPH/BSA. KRPH buffer was removed, and cells were incubated for 20 min with 170 μL of 100 nM insulin diluted in KRBH buffer; then, 19 μL of 10 mM 2-deoxy-D-glucose (Sigma-Aldrich) was added and the cells were incubated for 20 min. Cells were then washed four times with cold PBS and lysed with 60 μL of reagent I of the Glucofax kit. After 60 min of incubation at 37 °C, 20 μL of cell lysates was collected and transferred into a white 96-well plate. Then, 100 μL of reagent II was added, and after 10 min of incubation, the chemiluminescence was recorded on the EnSight multimode reader (PerkinElmer). Experiments were performed three times in sextuplet.

Real-Time PCR Analysis. Total RNA was extracted using a NucleoSpin RNA kit (Macherey-Nagel, Hoerdt, France), and cDNA was synthesized from 0.5 μg of RNA using Moloney murine leukemia virus reverse transcriptase (Thermo Fisher Scientific) and used for PCR amplification. Real-time PCR (RT-PCR) was performed on the LightCycler 480 instrument (Roche Applied Science, Basel, Switzerland) using the EvaGreen master mix (Euromedex, Souffelweyersheim, France). The comparative Ct method ($2^{-(\Delta\Delta Ct)}$) was used to calculate the relative differences in mRNA expression. The acidic ribosomal phosphoprotein P0 (*Rplp0*) was used as the housekeeping gene. Changes were normalized to the mean of control values, which was set to 1. Primers were synthesized by Eurogentec (Seraing, Belgium), and their sequences were previously published.[17,36,42] Experiments were performed five times in duplicate.

MitoTracker Staining. 3T3-L1 adipocytes were trypsinized and centrifuged at 300*g* at 4 °C for 5 min. Cells were suspended in KRPH containing 0.5% BSA and incubated with 0.1 μM MitoTracker Green FM (Thermo Fisher Scientific) for 30 min at 37 °C. Cells were spun at 300*g* at 4 °C for 5 min and suspended in 400 μL of fresh KRPH; then, 50,000 cells were analyzed using a BD Accuri C6 flow cytometer (BD Biosciences). Experiments were performed three times in triplicate.

Cell-Based PPAR and RXRα Transactivation Assay. The *PPARγ-LBD-Gal4* or *PPARα-LBD-Gal4* expression vector (given by Dr. Teruo Kawada, Kyoto University, Japan) was transfected along with the SV40-driven Renilla luciferase expression vector in HEK293 cells stably expressing the Gal4 response element-driven Firefly luciferase reporter (pGL4.35[luc2P/9XGAL4UAS/Hygro] vector from Promega, Madison, WI, USA). Thirty-six hours after trans-

https://dx.doi.org/10.1021/acs.jmedchem.0c01555
J. Med. Chem. XXXX, XXX, XXX−XXX

fection, cells were exposed to the tested compounds for additional 16 h; then, Firefly and Renilla luciferase activities were measured in the cell lysates using the reagents Genofax A and C (Yelen) in an EnSight multimode reader (PerkinElmer). PPAR transactivation activity of the compounds is calculated as the ratio of Firefly to Renilla luciferase activity. Experiments were performed at least three times in duplicate (allowing the calculation of EC_{50} and maximal activation, Table 1), and a representative experiment is shown in Figure 3 and Figure S5. For the measure of PPARδ transactivation, HG5LN-GAL-PPARδ reporter cell line was previously described.[44] Reporter cells were seeded at a density of 20,000 cells well^{-1} in 96-well white opaque tissue culture plates and maintained in phenol red-free Dulbecco's modified Eagle's medium (DMEM) supplemented with 5% dextran-coated, charcoal-treated fetal calf serum. Twenty-four later, the culture medium was replaced with DMEM containing tested compounds. After 16 h, exposure media were replaced with media containing 0.3 mM luciferin. Luminescence was measured in intact living cells for 2 s in a MicroBeta Wallac luminometer (PerkinElmer). Experiments were performed twice in duplicate. The measurement of RXRα transactivation was performed as described for PPARγ except that the *RXRα-LBD-Gal4* expression vector was transfected.

Mammalian Two-Hybrid Assay. HEK293 cells stably expressing the GAL4 response element-driven Firefly luciferase reporter were transfected with the SV40-driven Renilla luciferase expression vector together with the expression vector of a fusion protein of the VP16 activation domain to PPARγ-LBD and with the expression vector of a fusion protein of the GAL4-DNA binding domain to NCoR1, SMRT, TIF2, MED1, or RXRα. Then, cells were treated as described for the cell-based PPAR transactivation assay. Experiments were performed two to three times in duplicate.

Immunoblot. 3T3-L1 adipocytes were incubated 24 h with 1% SVF and then treated with PPARγ agonists for 60 min followed by 90 min of stimulation with murine TNF (50 ng mL^{-1}). Cells were lysed in the presence of a cocktail of protease and phosphatase inhibitor. Identical amounts of total protein were heat-denatured and reduced (70 °C; 10 min), then submitted to SDS-PAGE separation on 4−12% gradient (Thermo Fisher Scientific), and transferred to polyvinylidene fluoride membranes. Membranes were blocked for 1 h in 5% BSA solution and incubated with the appropriate primary and HRP-conjugated secondary antibodies (1/1000 and 1/10,000 dilutions, respectively). Immunodetections were performed using the ECL reagent, and image acquisition was performed by using a chemiluminescent CCD imager ImageQuant LAS 4000 (GE Healthcare, Velizy-Villacoublay, France).

Measure of *In Vitro* PPARγ Phosphorylation. *In vitro* phosphorylation was performed on wild-type PPARγ in the apo form and in complex with **7j** and Rosi. Stock solutions of ligands were prepared by diluting with 100% DMSO to a concentration of 50 mM. The stock solutions were further diluted with 50 mM Tris−HCl (pH 7.5) up to the final concentrations of 0.1, 1, and 10 μM and pre-equilibrated overnight at 4 °C with the protein. Phosphorylation was carried out at 30 °C for 3.5 h in 300 μL of buffer containing 50 mM Tris−HCl (pH 7.5), 7.2 μg mL^{-1} PPARγ, 0.1 μM, 1 μM, 10 μM ligand, 25 mM $MgCl_2$, 50 μM DTT, 2 mM ATP, and 0.66 ng mL^{-1} CDK5/p35 (Sigma-Aldrich code no. SRP5011). Then, polystyrene microwell plates were coated overnight at 4 °C with the reaction mixture, then washed three times with PBS + Tween 0.005%, and left to block in PBS containing 1% bovine serum for 90 min at 37 °C. The wells were washed three times and incubated for 60 min at 37 °C with 100 μL of antiphospho-Ser/The-Pro antibody (SigmaAldrich code no. A05368) diluted 1/500 in PBS. After three washes, 100 μL of antimouse IgG-peroxidase antibody produced in goat (Sigma Aldrich code no. A4416; 1/1000 in PBS) were added to the wells and incubated 60 min at 37 °C. The wells were washed, and 200 μL of *o*-phenylenediamine dihydrochloride (SIGMAFAST OPD code no. P9187) dissolved in water was added to the wells. Optical density was measured at 450 nm using an ApplyScan Thermo Fisher reader, and the data were processed using Excel.

Experiments were performed three times in triplicates.

Protein Expression and Purification. PPARγ LBD was expressed as N-terminal His-tagged proteins using a pET28 vector and purified as previously described.[45] Briefly, freshly transformed *Escherichia coli* BL21 DE3 were grown in the LB medium with 30 μg of kanamycin mL^{-1} at 310 K to an OD of 0.6. The culture was then induced with 0.2 mM isopropyl-β-D-thio-galactopyranoside and further incubated at 291 K for 20 h. Cells were harvested and resuspended in a 20 mL L^{-1} culture of buffer A (20 mM Tris−HCl, 150 mM NaCl, 10% glycerol, 1 mM Tris 2-carboxyethylphosphine HCL (TCEP), pH 8) in the presence of protease inhibitors (cOmplete Mini EDTA-free; Roche Applied Science). Cells were sonicated, and the soluble fraction was isolated by centrifugation (35,000*g* for 45 min). The supernatant was loaded onto a Ni^{2+}-nitrilotriacetic acid column (GE Healthcare) and eluted with a gradient of imidazole 0−500 mM in buffer A (20 mM Tris−HCl, 20 mM NaCl, 10% glycerol, 1 mM TCEP, pH 8) (batch method). The pure protein was identified by SDS PAGE. The protein was then dialyzed over buffer A to remove imidazole, and it was cleaved with thrombin protease (Sigma-Aldrich Life Science) (10 units mg^{-1}) at room temperature for 2 h. The digested mixture was reloaded onto a Ni^{2+}-nitrilotriacetic acid column to remove the His tag and the undigested protein. The flow-through was dialyzed with buffer B (20 mM Tris−HCl, 10% glycerol, 1 mM TCEP, pH 8) to remove NaCl, loaded onto a Q Sepharose HP column (GE Healthcare), and eluted with a gradient of NaCl 0−500 mM in buffer B with a BioLogic DuoFlow FPLC system (Bio-Rad Laboratories, Italy). Finally, the protein was purified by gel filtration chromatography on a HiLoad Superdex 75 column (GE Healthcare) and eluted with buffer C (20 mM Tris−HCl, 1 mM TCEP, 0.5 mM EDTA, pH 8). The protein was then concentrated at 8 mg mL^{-1} using Amicon centrifugal concentrators with a 10 kDa cutoff membrane (Millipore, USA).

Crystallization and Data Collection. Crystals of apo-PPARγ were obtained by vapor diffusion at 18 °C using a sitting drop made by mixing 2 μL of protein solution with 2 μL of reservoir solution (0.8 M Na citrate, 0.15 M Tris, pH 8.0). The crystals were soaked for 3 days in a storage solution (1.2 M Na citrate, 0.15 M Tris, pH 8.0) containing the ligand **7j** or **7a** (0.5 mM). The ligand dissolved in DMSO (50 mM) was diluted in the storage solution so that the final concentration of DMSO was 1%. The storage solution with glycerol 20% (v/v) was used as the cryoprotectant. Crystals (0.15 × 0.15 mm) of PPARγ/**7j** and PPARγ/**7a** belong to the space group *C*2 with cell parameters shown in Table S1.

Structure Determination and Refinement. X-ray data sets were collected at 100 K under a nitrogen stream using synchrotron radiation (beamline ID30B at ESRF, Grenoble, France). The collected data were processed using the programs Mosflm and Scala.[46] Structure solution was performed with AMoRe,[47] using the coordinates of PPARγ/LT175R (27) (PDB code: 3D6D) as the starting model. The coordinates were then refined with CNS[48] and with PHENIX[49] including data between 58.2 and 2.0 Å for PPARγ/**7j** (57.4−1.8 Å for PPARγ/**7a**). The statistics of crystallographic data and refinement is summarized in Table S1. The coordinates and structure factors described here have been deposited in the PDB under accession numbers 6QJ5 and 6ZLY for PPARγ/**7j** and PPARγ/**7a**, respectively.

Surface Plasmon Resonance. Surface plasmon resonance analyses were performed by using a Pioneer AE optical biosensor equipped with COOH5 chips (SensiQ). PPARγ surfaces were prepared by using standard amine-coupling procedures[50] and HBS (Hepes-buffered saline: 10 mM Hepes, 150 mM NaCl, 0.005% P20, DMSO 1%, pH 7.4) as the running buffer. Flow cells were activated for 7 min by injecting 140 μL of 50 mM *N*-hydroxysuccinimide (NHS)/200 mM ethyl-3(3-dimethylamino) propylcarbodiimide (EDC). A 0.25 mg mL^{-1} PPARγ solution (150 μL, in 10 mM NaOAc, pH 5.0) was injected for 15 min at 10 μL min^{-1} on channels 1 and 3 (channel 2 was used as the reference, for a duplicate experiment) followed by a 70 μL injection of ethanolamine to block any remaining activated groups on the surface. RU (11,320 and 11,220) of protein was immobilized on channels 1 and 3,

https://dx.doi.org/10.1021/acs.jmedchem.0c01555
J. Med. Chem. XXXX, XXX, XXX−XXX

respectively. The screening of the analytes was performed using HBS, with 1% DMSO. To collect details, a dilution protocol was used, injecting different concentrations of the analytes at a flow rate of 50 μL min^{-1} over the two channels at 20 °C (association phase of 60 s). A similar protocol was followed for the experiments with PPARα, using a PCH chip (Pall ForteBio).

Four buffer blanks were injected for double referencing. The regeneration of the surfaces between binding cycles was not necessary because all the analytes dissociate quickly in the 120 s dissociation phase. A DMSO calibration plot was constructed (buffer sample containing 0−2% (vol/vol) DMSO) to correct for bulk refractive index shifts. All sensorgrams were processed by using double referencing. To obtain kinetic rate constants and affinity constants, the corrected response data were fit in the program QDAT. A kinetic analysis of each ligand/analyte interaction was obtained by fitting the response data to a 1/1 bimolecular interaction model. The equilibrium dissociation constant (K_d) was determined by the ratio of k_{off}/k_{on}.

Statistical Analyses. Statistical significance was estimated with one-way ANOVA followed by the Bonferroni or Dunnett post-hoc test, with the two-tailed *t*-test or with the *F*-test (statistical test is specified in figure legends) using GraphPad Prism version 5.0 (GraphPad Software, San Diego, CA). Differences with *p* values of less than 0.05 were considered statistically significant.

■ ASSOCIATED CONTENT

Supporting Information

The Supporting Information is available free of charge at https://pubs.acs.org/doi/10.1021/acs.jmedchem.0c01555.

PDB data of the compounds (PDB)

NMR and HPLC spectra of **3a**, **7a**, and **7j**; X-ray crystal structures of **3a**, **7a**, **7j**, rosiglitazone and SR2067 in PPARγ LBD; SPR sensorgrams of **3a**, **7a**, and **7j**; adipogenic effect of the compounds; PPARγ, PPARδ, and RXRα transactivation; PPARγ/RXRα heterodimerization; toxicity of **7j**; statistics of crystallographic data and refinement (PDF)

Molecular formula string for **3a**, **7a**, and **7j** (CSV)

■ AUTHOR INFORMATION

Corresponding Author

Franck Peiretti − *Aix Marseille University, INSERM, INRAE, C2VN, 13385 Marseille, France;* orcid.org/0000-0001-7198-0534; Email: franck.peiretti@univ-amu.fr

Authors

Roberta Montanari − *Istituto di Cristallografia, Consiglio Nazionale delle Ricerche, 00015 Rome, Italy*

Davide Capelli − *Istituto di Cristallografia, Consiglio Nazionale delle Ricerche, 00015 Rome, Italy*

Bernadette Bonardo − *Aix Marseille University, INSERM, INRAE, C2VN, 13385 Marseille, France*

Cécilia Colson − *Université Côte d'Azur, CNRS, Inserm, iBV, 06108 Nice, France*

Ez-Zoubir Amri − *Université Côte d'Azur, CNRS, Inserm, iBV, 06108 Nice, France*

Marina Grimaldi − *Institut de Recherche en Cancérologie de Montpellier (IRCM), INSERM, University of Montpellier, ICM, 34298 Montpellier, France*

Patrick Balaguer − *Institut de Recherche en Cancérologie de Montpellier (IRCM), INSERM, University of Montpellier, ICM, 34298 Montpellier, France*

Keiichi Ito − *Laboratory of Biochemistry and Molecular Biology, The Rockefeller University, New York, New York 10065, United States*

Robert G. Roeder − *Laboratory of Biochemistry and Molecular Biology, The Rockefeller University, New York, New York 10065, United States*

Giorgio Pochetti − *Istituto di Cristallografia, Consiglio Nazionale delle Ricerche, 00015 Rome, Italy;* orcid.org/0000-0002-3980-3180

Jean Michel Brunel − *Aix Marseille University, INSERM, SSA, MCT, 13385 Marseille, France;* orcid.org/0000-0002-9355-8980

Complete contact information is available at: https://pubs.acs.org/10.1021/acs.jmedchem.0c01555

Author Contributions

$^{\nabla}$F.P. and R.M. contributed equally to this work; G.P. and J.M.B. contributed equally to this work.

Notes

The authors declare no competing financial interest.

Coordinates and structure factors of the PPARγ complexes with the compounds **7j** and **7a** have been deposited in the Protein Data Bank under the accession codes 6QJ5 and 6ZLY, respectively. Authors will release the atomic coordinates and experimental data upon article publication.

Genes are identified by the symbols approved by the Human Genome Organization.

■ ACKNOWLEDGMENTS

This work was supported by funds from Aix Marseille University, Inserm, CNRS, ANR and National Institutes of Health grant DK071900 to R.G.R.

■ ABBREVIATIONS

BOP, benzotriazol-1-yloxytris(dimethylamino)phosphonium hexafluorophosphate; CDK5, cyclin-dependent kinase 5; hMADS, human multipotent adipose-derived Stem; LBD, ligand binding domain; NAFLD, nonalcoholic fatty liver disease; PPRE, PPAR responsive element; Rosi, rosiglitazone; SPPARγMs, selective PPARγ modulators

■ REFERENCES

(1) Braissant, O.; Foufelle, F.; Scotto, C.; Dauça, M.; Wahli, W. Differential Expression of Peroxisome Proliferator-Activated Receptors (PPARs): Tissue Distribution of PPAR-Alpha, -Beta, and -Gamma in the Adult Rat. *Endocrinology* **1996**, *137*, 354−366.

(2) Botta, M.; Audano, M.; Sahebkar, A.; Sirtori, C. R.; Mitro, N.; Ruscica, M. PPAR Agonists and Metabolic Syndrome: An Established Role? *Int. J. Mol. Sci.* **2018**, *19*, 1197.

(3) Derosa, G.; Sahebkar, A.; Maffioli, P. The Role of Various Peroxisome Proliferator-Activated Receptors and Their Ligands in Clinical Practice. *J. Cell. Physiol.* **2018**, *233*, 153−161.

(4) Silva, A. K. S.; Peixoto, C. A. Role of Peroxisome Proliferator-Activated Receptors in Non-Alcoholic Fatty Liver Disease Inflammation. *Cell. Mol. Life Sci.* **2018**, *75*, 2951−2961.

(5) Pawlak, M.; Lefebvre, P.; Staels, B. Molecular Mechanism of PPARα Action and Its Impact on Lipid Metabolism, Inflammation and Fibrosis in Non-Alcoholic Fatty Liver Disease. *J. Hepatol.* **2015**, *62*, 720−733.

(6) Tsunoda, F.; Asztalos, I. B.; Horvath, K. V.; Steiner, G.; Schaefer, E. J.; Asztalos, B. F. Fenofibrate, HDL, and Cardiovascular Disease in Type-2 Diabetes: The DAIS Trial. *Atherosclerosis* **2016**, *247*, 35−39.

(7) Yaghoubi, M.; Jafari, S.; Sajedi, B.; Gohari, S.; Akbarieh, S.; Heydari, A. H.; Jameshoorani, M. Comparison of Fenofibrate and Pioglitazone Effects on Patients with Nonalcoholic Fatty Liver Disease. *Eur. J. Gastroenterol. Hepatol.* **2017**, *29*, 1385−1388.

(8) Davidson, M. H.; Armani, A.; McKenney, J. M.; Jacobson, T. A. Safety Considerations with Fibrate Therapy. *Am. J. Cardiol.* **2007**, *99*, 3C−S18.
(9) Ida, S.; Kaneko, R.; Murata, K. Efficacy and Safety of Pemafibrate Administration in Patients with Dyslipidemia: A Systematic Review and Meta-Analysis. *Cardiovasc. Diabetol.* **2019**, *18*, 38.
(10) Liu, Y.; Colby, J. K.; Zuo, X.; Jaoude, J.; Wei, D.; Shureiqi, I. The Role of PPAR-δ in Metabolism, Inflammation, and Cancer: Many Characters of a Critical Transcription Factor. *Int. J. Mol. Sci.* **2018**, *19*, 3339.
(11) Wu, C.-C.; Baiga, T. J.; Downes, M.; La Clair, J. J.; Atkins, A. R.; Richard, S. B.; Fan, W.; Stockley-Noel, T. A.; Bowman, M. E.; Noel, J. P.; Evans, R. M. Structural Basis for Specific Ligation of the Peroxisome Proliferator-Activated Receptor δ. *Proc. Natl. Acad. Sci. U. S. A.* **2017**, *114*, E2563−E2570.
(12) Olefsky, J. M. Treatment of Insulin Resistance with Peroxisome Proliferator-Activated Receptor Gamma Agonists. *J. Clin. Invest.* **2000**, *106*, 467−472.
(13) Abbas, A.; Blandon, J.; Rude, J.; Elfar, A.; Mukherjee, D. PPAR- γ Agonist in Treatment of Diabetes: Cardiovascular Safety Considerations. *Cardiovasc. Hematol. Agents Med. Chem.* **2012**, *10*, 124−134.
(14) Kung, J.; Henry, R. R. Thiazolidinedione Safety. *Expert Opin. Drug Saf.* **2012**, *11*, 565−579.
(15) Balint, B. L.; Nagy, L. Selective Modulators of PPAR Activity as New Therapeutic Tools in Metabolic Diseases. *Endocr., Metab. Immune Disord.: Drug Targets* **2006**, *6*, 33−43.
(16) Higgins, L. S.; Depaoli, A. M. Selective Peroxisome Proliferator-Activated Receptor Gamma (PPARgamma) Modulation as a Strategy for Safer Therapeutic PPARgamma Activation. *Am. J. Clin. Nutr.* **2010**, *91*, 267S−272S.
(17) Choi, J. H.; Banks, A. S.; Estall, J. L.; Kajimura, S.; Boström, P.; Laznik, D.; Ruas, J. L.; Chalmers, M. J.; Kamenecka, T. M.; Blüher, M.; Griffin, P. R.; Spiegelman, B. M. Anti-Diabetic Drugs Inhibit Obesity-Linked Phosphorylation of PPARgamma by Cdk5. *Nature* **2010**, *466*, 451−456.
(18) Choi, J. H.; Banks, A. S.; Kamenecka, T. M.; Busby, S. A.; Chalmers, M. J.; Kumar, N.; Kuruvilla, D. S.; Shin, Y.; He, Y.; Bruning, J. B.; Marciano, D. P.; Cameron, M. D.; Laznik, D.; Jurczak, M. J.; Schürer, S. C.; Vidović, D.; Shulman, G. I.; Spiegelman, B. M.; Griffin, P. R. Antidiabetic Actions of a Non-Agonist PPARγ Ligand Blocking Cdk5-Mediated Phosphorylation. *Nature* **2011**, *477*, 477−481.
(19) Balakumar, P.; Mahadevan, N.; Sambathkumar, R. A Contemporary Overview of PPARα/γ Dual Agonists for the Management of Diabetic Dyslipidemia. *Curr. Mol. Pharmacol.* **2019**, *12*, 195−201.
(20) Fiévet, C.; Fruchart, J.-C.; Staels, B. PPARalpha and PPARgamma Dual Agonists for the Treatment of Type 2 Diabetes and the Metabolic Syndrome. *Curr. Opin. Pharmacol.* **2006**, *6*, 606−614.
(21) Jani, R. H.; Pai, V.; Jha, P.; Jariwala, G.; Mukhopadhyay, S.; Bhansali, A.; Joshi, S. A Multicenter, Prospective, Randomized, Double-Blind Study to Evaluate the Safety and Efficacy of Saroglitazar 2 and 4 Mg Compared with Placebo in Type 2 Diabetes Mellitus Patients Having Hypertriglyceridemia Not Controlled with Atorvastatin Therapy (PRESS VI). *Diabetes Technol. Ther.* **2014**, *16*, 63−71.
(22) Pai, V.; Paneerselvam, A.; Mukhopadhyay, S.; Bhansali, A.; Kamath, D.; Shankar, V.; Gambhire, D.; Jani, R. H.; Joshi, S.; Patel, P. A Multicenter, Prospective, Randomized, Double-Blind Study to Evaluate the Safety and Efficacy of Saroglitazar 2 and 4 Mg Compared to Pioglitazone 45 Mg in Diabetic Dyslipidemia (PRESS V). *J Diabetes Sci Technol* **2014**, *8*, 132−141.
(23) Giampietro, L.; Laghezza, A.; Cerchia, C.; Florio, R.; Recinella, L.; Capone, F.; Ammazzalorso, A.; Bruno, I.; De Filippis, B.; Fantacuzzi, M.; Ferrante, C.; Maccallini, C.; Tortorella, P.; Verginelli, F.; Brunetti, L.; Cama, A.; Amoroso, R.; Loiodice, F.; Lavecchia, A. Novel Phenyldiazenyl Fibrate Analogues as PPAR $\alpha/\gamma/\delta$ Pan-Agonists for the Amelioration of Metabolic Syndrome. *ACS Med. Chem. Lett.* **2019**, *10*, 545−551.
(24) Laghezza, A.; Piemontese, L.; Cerchia, C.; Montanari, R.; Capelli, D.; Giudici, M.; Crestani, M.; Tortorella, P.; Peiretti, F.; Pochetti, G.; Lavecchia, A.; Loiodice, F. Identification of the First PPARα/γ Dual Agonist Able To Bind to Canonical and Alternative Sites of PPARγ and To Inhibit Its Cdk5-Mediated Phosphorylation. *J. Med. Chem.* **2018**, *61*, 8282−8298.
(25) Xu, H.-R.; Zhang, J.-W.; Chen, W.-L.; Ning, Z.-Q.; Li, X.-N. Pharmacokinetics, Safety and Tolerability of Chiglitazar, A Novel Peroxisome Proliferator-Activated Receptor (PPAR) Pan-Agonist, in Healthy Chinese Volunteers: A Phase I Study. *Clin. Drug Invest.* **2019**, *39*, 553−563.
(26) Gim, H. J.; Choi, Y.-S.; Li, H.; Kim, Y.-J.; Ryu, J.-H.; Jeon, R. Identification of a Novel PPAR-γ Agonist through a Scaffold Tuning Approach. *Int. J. Mol. Sci.* **2018**, *19*, 3032.
(27) Guasch, L.; Sala, E.; Valls, C.; Blay, M.; Mulero, M.; Arola, L.; Pujadas, G.; Garcia-Vallvé, S. Structural Insights for the Design of New PPARgamma Partial Agonists with High Binding Affinity and Low Transactivation Activity. *J. Comput.-Aided Mol. Des.* **2011**, *25*, 717−728.
(28) Montanari, R.; Capelli, D.; Yamamoto, K.; Awaishima, H.; Nishikata, K.; Barendregt, A.; Heck, A. J. R.; Loiodice, F.; Altieri, F.; Paiardini, A.; Grottesi, A.; Pirone, L.; Pedone, E.; Peiretti, F.; Brunel, J. M.; Itoh, T.; Pochetti, G. Insights into PPARγ Phosphorylation and Its Inhibition Mechanism. *J. Med. Chem.* **2020**, *63*, 4811−4823.
(29) van Marrewijk, L. M.; Polyak, S. W.; Hijnen, M.; Kuruvilla, D.; Chang, M. R.; Shin, Y.; Kamenecka, T. M.; Griffin, P. R.; Bruning, J. B. SR2067 Reveals a Unique Kinetic and Structural Signature for PPARγ Partial Agonism. *ACS Chem. Biol.* **2016**, *11*, 273−283.
(30) Eliasson, B.; Smith, U.; Mullen, S.; Cushman, S. W.; Sherman, A. S.; Yang, J. Amelioration of Insulin Resistance by Rosiglitazone Is Associated with Increased Adipose Cell Size in Obese Type 2 Diabetic Patients. *Adipocyte* **2014**, *3*, 314−321.
(31) Liu, C.; Feng, T.; Zhu, N.; Liu, P.; Han, X.; Chen, M.; Wang, X.; Li, N.; Li, Y.; Xu, Y.; Si, S. Identification of a Novel Selective Agonist of PPARγ with No Promotion of Adipogenesis and Less Inhibition of Osteoblastogenesis. *Sci. Rep.* **2015**, *5*, 9530.
(32) Mukherjee, R.; Hoener, P. A.; Jow, L.; Bilakovics, J.; Klausing, K.; Mais, D. E.; Faulkner, A.; Croston, G. E.; Paterniti, J. R., Jr. A Selective Peroxisome Proliferator-Activated Receptor-Gamma (PPARgamma) Modulator Blocks Adipocyte Differentiation but Stimulates Glucose Uptake in 3T3-L1 Adipocytes. *Mol. Endocrinol.* **2000**, *14*, 1425−1433.
(33) Wu, J.; Cohen, P.; Spiegelman, B. M. Adaptive Thermogenesis in Adipocytes: Is Beige the New Brown? *Genes Dev.* **2013**, *27*, 234−250.
(34) Ohno, H.; Shinoda, K.; Spiegelman, B. M.; Kajimura, S. PPARγ Agonists Induce a White-to-Brown Fat Conversion through Stabilization of PRDM16 Protein. *Cell Metab.* **2012**, *15*, 395−404.
(35) Vernochet, C.; Peres, S. B.; Davis, K. E.; McDonald, M. E.; Qiang, L.; Wang, H.; Scherer, P. E.; Farmer, S. R. C/EBPalpha and the Corepressors CtBP1 and CtBP2 Regulate Repression of Select Visceral White Adipose Genes during Induction of the Brown Phenotype in White Adipocytes by Peroxisome Proliferator-Activated Receptor Gamma Agonists. *Mol. Cell. Biol.* **2009**, *29*, 4714−4728.
(36) Wu, J.; Boström, P.; Sparks, L. M.; Ye, L.; Choi, J. H.; Giang, A.-H.; Khandekar, M.; Virtanen, K. A.; Nuutila, P.; Schaart, G.; Huang, K.; Tu, H.; van Marken Lichtenbelt, W. D.; Hoeks, J.; Enerbäck, S.; Schrauwen, P.; Spiegelman, B. M. Beige Adipocytes Are a Distinct Type of Thermogenic Fat Cell in Mouse and Human. *Cell* **2012**, *150*, 366−376.
(37) Lin, J.; Handschin, C.; Spiegelman, B. M. Metabolic Control through the PGC-1 Family of Transcription Coactivators. *Cell Metab.* **2005**, *1*, 361−370.
(38) Pisani, D. F.; Djedaini, M.; Beranger, G. E.; Elabd, C.; Scheideler, M.; Ailhaud, G.; Amri, E.-Z. Differentiation of Human

https://dx.doi.org/10.1021/acs.jmedchem.0c01555
J. Med. Chem. XXXX, XXX, XXX−XXX

Adipose-Derived Stem Cells into "Brite" (Brown-in-White) Adipocytes. *Front. Endocrinol.* **2011**, *2*, 87.
(39) Guo, L.; Zhang, L.; Sun, Y.; Muskhelishvili, L.; Blann, E.; Dial, S.; Shi, L.; Schroth, G.; Dragan, Y. P. Differences in Hepatotoxicity and Gene Expression Profiles by Anti-Diabetic PPAR Gamma Agonists on Rat Primary Hepatocytes and Human HepG2 Cells. *Mol. Diversity* **2006**, *10*, 349−360.
(40) Germano, D.; Uteng, M.; Pognan, F.; Chibout, S.-D.; Wolf, A. Determination of Liver Specific Toxicities in Rat Hepatocytes by High Content Imaging during 2-Week Multiple Treatment. *Toxicol. In Vitro* **2015**, *30*, 79−94.
(41) Rachek, L. I.; Yuzefovych, L. V.; LeDoux, S. P.; Julie, N. L.; Wilson, G. L. Troglitazone, but Not Rosiglitazone, Damages Mitochondrial DNA and Induces Mitochondrial Dysfunction and Cell Death in Human Hepatocytes. *Toxicol. Appl. Pharmacol.* **2009**, *240*, 348−354.
(42) Elabd, C.; Chiellini, C.; Carmona, M.; Galitzky, J.; Cochet, O.; Petersen, R.; Pénicaud, L.; Kristiansen, K.; Bouloumié, A.; Casteilla, L.; Dani, C.; Ailhaud, G.; Amri, E.-Z. Human Multipotent Adipose-Derived Stem Cells Differentiate into Functional Brown Adipocytes. *Stem Cells* **2009**, *27*, 2753−2760.
(43) Vidal, N.; Cavaillé, J. P.; Poggi, M.; Peiretti, F.; Stocker, P. A Nonradioisotope Chemiluminescent Assay for Evaluation of 2-Deoxyglucose Uptake in 3T3-L1 Adipocytes. Effect of Various Carbonyls Species on Insulin Action. *Biochimie* **2012**, *94*, 2569−2576.
(44) Seimandi, M.; Lemaire, G.; Pillon, A.; Perrin, A.; Carlavan, I.; Voegel, J. J.; Vignon, F.; Nicolas, J.-C.; Balaguer, P. Differential Responses of PPARalpha, PPARdelta, and PPARgamma Reporter Cell Lines to Selective PPAR Synthetic Ligands. *Anal. Biochem.* **2005**, *344*, 8−15.
(45) Pochetti, G.; Godio, C.; Mitro, N.; Caruso, D.; Galmozzi, A.; Scurati, S.; Loiodice, F.; Fracchiolla, G.; Tortorella, P.; Laghezza, A.; Lavecchia, A.; Novellino, E.; Mazza, F.; Crestani, M. Insights into the Mechanism of Partial Agonism: Crystal Structures of the Peroxisome Proliferator-Activated Receptor Gamma Ligand-Binding Domain in the Complex with Two Enantiomeric Ligands. *J. Biol. Chem.* **2007**, *282*, 17314−17324.
(46) Kabsch, W. XDS. *Acta Cryst.* **2010**, *66*, 125−132.
(47) Navaza, J. AMoRe: An Automated Package for Molecular Replacement. *Acta Cryst A* **1994**, *50*, 157−163.
(48) Brünger, A. T.; Adams, P. D.; Clore, G. M.; DeLano, W. L.; Gros, P.; Grosse-Kunstleve, R. W.; Jiang, J. S.; Kuszewski, J.; Nilges, M.; Pannu, N. S.; Read, R. J.; Rice, L. M.; Simonson, T.; Warren, G. L. Crystallography & NMR System: A New Software Suite for Macromolecular Structure Determination. *Acta Cryst.* **1998**, *54*, 905−921.
(49) Adams, P. D.; Afonine, P. V.; Bunkóczi, G.; Chen, V. B.; Davis, I. W.; Echols, N.; Headd, J. J.; Hung, L.-W.; Kapral, G. J.; Grosse-Kunstleve, R. W.; McCoy, A. J.; Moriarty, N. W.; Oeffner, R.; Read, R. J.; Richardson, D. C.; Richardson, J. S.; Terwilliger, T. C.; Zwart, P. H. PHENIX: A Comprehensive Python-Based System for Macromolecular Structure Solution. *Acta Cryst.* **2010**, *66*, 213−221.
(50) Jonsson, U.; Malmqvist, M. Real Time Biospecific Interaction Analysis. The Integration of Surface Plasmon Resonance Detection, General Biospecific Interface Chemistry and Microfluides into One Analytical System. In *Advances in Biosensor*, Turner, A. ed.; JAI Press: San Diego, 1992; pp. 291−336.

https://dx.doi.org/10.1021/acs.jmedchem.0c01555
J. Med. Chem. XXXX, XXX, XXX−XXX